

# High Pressure Investigations on $A^I B^{III}$ Zintl Compounds ( $A^I = \text{Li to Cs}$ ; $B^{III} = \text{Al to Tl}$ ) up to 30 GPa

Jürgen Evers

**Abstract** For the AIBIII compounds ( $AI = \text{Li to Cs}$ ;  $BIII = \text{Al to Tl}$ ) the stabilities of the NaTl- and the  $\beta$ -brass-type structures have been calculated by density functional theory (DFT) with the program WIEN2k. In agreement with the experimental data obtained at 1 bar LiAl, LiGa, NaIn and NaTl are stable with the NaTl-type structure, LiTl with the  $\beta$ -brass-type structure. Interestingly, LiIn with the NaTl-type structure is high temperature phase and LiIn with the  $\beta$ -brass-type structure is low temperature phase. For the 14 remaining AIBIII compounds the endothermic formation energies at 0 K and 0 bar have been estimated for the NaTl-type structure phases. In addition, the high pressure range is estimated to obtain such phases in the diamond anvil cell. For LiTl, NaTl, KTI, RbTl, and CsTl the results of high pressure investigations in the diamond anvil cell up to 30 GPa are reported. The near-neighbor-diagram for the AIBIII compounds with the NaTl-type structure has been calculated.

**Keywords**  $\beta$ -brass-type structure · DFT calculation · Diamond anvil cell · High pressure transformation · NaTl-type structure · Zintl compounds

## Contents

1	Introduction .....	58
2	Apparatus and Experimental Techniques .....	60
3	Computational Methods .....	61
4	Crystal Structures .....	63
4.1	NaTl-Type Structure .....	64
4.2	$\beta$ -Brass-Type Structure .....	64
4.3	Tetragonal Distorted NaTl-Type Structure .....	65
4.4	AuCu-Type Structure .....	66

5	Results and Discussion .....	66
5.1	Aluminides LiAl, NaAl, KAl, RbAl, and CsAl .....	67
5.2	Gallides LiGa, NaGa, KGa, RbGa, and CsGa .....	71
5.3	Indides LiIn, NaIn, KIn, RbIn, and CsIn .....	74
5.4	Thallides LiTl, NaTl, KTI, RbTl, and CsTl .....	79
6	Conclusion .....	93
	References .....	95

## 1 Introduction

Zintl compounds are introduced as solids with a quite unique hybrid of chemical bonding. In the Zintl concept, it is assumed that in such compounds electrons are transferred from the electropositive to the electronegative constituent. By this electron transfer, the valence shell of the electronegative constituent is filled. As a result, covalent bonding in the anionic partial structure obeys then the (8-N) rule for normal valence compounds. NaTl is the prototype of Zintl compounds. Four additional  $A^I B^{III}$  compounds (LiAl, LiGa, LiIn, NaIn) with the NaTl-type structure were characterized by Zintl in the 1930s of the last century. Nevertheless, one  $A^I B^{III}$  compound, LiTl, crystallized in the alloy structure of  $\beta$ -brass. This structural concurrence interested the theoreticians, performing density-functional theory (DFT) calculations on such compounds, however, only on the six known ones. With KTI, synthesized in 1999 at high pressure (HP) of 2 GPa in a diamond anvil cell (DAC) by Evers and Oehlinger, a new access to such compounds was opened. In this study, the results are reported on DFT calculations for the whole 20  $A^I B^{III}$  compounds ( $A^I = \text{Li to Cs}$ ;  $B^{III} = \text{Al to Tl}$ ), and, furthermore, the results of in situ HP experiments in a DAC up to 30 GPa presented for the thallides LiTl, NaTl, KTI, RbTl, and CsTl.

In the huge field of intermetallic phases, Zintl compounds are a class of solids formed by electropositive with electronegative constituents. Such polar compounds have definite compositions and a quite unique bonding hybrid with ionic, covalent, and metallic contributions. In the Zintl concept [1–6], it is assumed that valence electrons are transferred from the electropositive to the electronegative constituent. By this electron transfer, the valence shells of the electronegative partner are filled, thus forming covalent bonds. This covalent bonding in the anionic partial structure obeys the (8-N) rule of normal valence compounds. Hoffmann assigned this simple concept as the “single most important theoretical concept in solid-state chemistry of the 20th century” [7] “It forges a link between solid-state chemistry and organic, or main group chemistry” [7].

The compound NaTl [8] is considered as the prototype of Zintl phases [9], although the triel element thallium lies left to the Zintl boundary [10]. This boundary was introduced by Laves [11] as dividing line between triel elements aluminum to thallium and tetrel elements silicon to lead. It was assumed that tetrel elements form salt-like compounds with electropositive metals, contrary to triel elements that generate alloy-like compounds. Due to modern structural and

electronic investigations on such compounds, especially by Corbett [10], this traditional distinction seems no longer appropriate.

NaTl, itself, crystallizes in the NaTl-type structure [8] (B32, Strukturbericht classification [12]). Assuming that one electron is transferred per formula unit (f.u.) from the electropositive  $A^I$  metal sodium to the more electronegative  $B^{III}$  element thallium,  $Tl^-$  ions become iso-valence-electronic with main group IV elements carbon to tin and build up a diamond-type partial structure with four homonuclear bonds, obeying the (8-N) rule. Zintl and coworkers prepared four additional  $A^I B^{III}$  compounds with the NaTl-type structure, such as NaIn [13], LiAl [1], LiGa [14], and LiIn [14]. However, in the homologous series of lithium compounds, LiTl [14] does not crystallize in the NaTl, but in the  $\beta$ -brass-type structure (B2, Strukturbericht classification [15]). As it will be shown later, the NaTl- and the  $\beta$ -brass-type alloy are closely related to each other, because they can be assigned as different binary varieties of a body-centered cubic (bcc) arrangement. They consist of interpenetrating cubes giving 8:8 nearest neighbor coordination for both.

The structural change from the NaTl- (B32) to the  $\beta$ -brass-type structure (B2), which is found when in the homologous  $A^I Tl$  series the metallic radius of the  $A^I$  metal is lowered from sodium to lithium, interested a lot of theoreticians. Magnovetskii and Krasko [16] calculated with Brillouin–Wigner perturbation theory a stabilization for LiAl and NaTl in the B32 and for LiTl in the B2 structure. Schmidt [9, 17] used the local density functional approach on the basis of the muffin tin model, to calculate the structural stability of the B32 and the B2 structures, however, only for the two compounds NaTl and LiTl. Christensen [18] calculated within the density-functional formalism with the local density approximation (LDA) the stability of B2 and B32 structures in  $A^I B^{III}$  compounds LiAl, LiGa, LiIn, LiTl, NaIn, and NaTl. Christensen confirmed by such calculations the stabilities at zero temperature and pressure [18], which Zintl had found experimentally in his classical works at room temperature and 1 bar. According to Christensen, LiAl, LiGa, LiIn, NaIn, and NaTl are stable in the B32, and LiTl in the B2 structure. However, for LiIn Christensen calculated that the structural B32–B2 difference is only  $-2$  mRy ( $-0.6$  kcal/mole). The results of Schmidt [9, 17] and Christensen [18] agreed in the relative stabilities for the structures of NaTl and LiTl, but differed slightly in their absolute energies.

In 2002, Ehrenberg et al. [19] prepared a low temperature modification of LiIn. At 170 K cubic LiIn with the NaTl-type structure, space group Fd-3m, was transformed in a reversible group–subgroup “translationengleich” transition into a tetragonal modification in space group  $I4_1/amd$ . The tetragonal distortion is with 0.5% very small, however, leading to a slightly more densely packing than in the cubic case. The first structural change at high pressure (HP) from the NaTl- into the  $\beta$ -brass-type structure was investigated in 1998 by Schwarz et al. [20]. Starting with LiIn with the NaTl-type structure, at 11 GPa the  $\beta$ -brass alloy structure was obtained. Together with LiTl, stable at ambient pressure, LiIn is the second  $A^I B^{III}$  phase with the  $\beta$ -brass-type structure. More than 60 years after Zintl’s classical works, Evers and Oehlinger prepared in 1999 with high pressure HP-KTl the first novel binary  $A^I B^{III}$  compound with the NaTl-type structure [21].

This compound was prepared at 2 GPa in a DAC from the normal pressure phase KTI which consists of isolated  $\text{TI}_6$ -octahedra [22].

The earlier published calculations had focused the interest to only six  $\text{A}^{\text{I}}\text{B}^{\text{III}}$  compounds, which were firstly synthesized by Zintl. However, combining five  $\text{A}^{\text{I}}$  metals (Li to Cs) with four  $\text{B}^{\text{III}}$  elements (Al to Tl) results in 20  $\text{A}^{\text{I}}\text{B}^{\text{III}}$  compounds. Therefore, Zintl's work, although complete at ambient pressure, is enlightening only for 30% of the whole  $\text{A}^{\text{I}}\text{B}^{\text{III}}$  series. However, in recent years with DACs, heated by a laser, preparative conditions are enlarged to 50 GPa and 1,000°C for routine chemical syntheses in solid-state chemistry. Indeed, there is now a chance to have a look on the 70% of the remaining  $\text{A}^{\text{I}}\text{B}^{\text{III}}$  compounds for the stability of the NaTI- or the  $\beta$ -brass-type structure or new structures. After the successful HP-synthesis of KTI, it seems that RbTI and CsTI of the thallide series could be also good candidates for stabilizing here the NaTI-type structure after a HP treatment.

In this chapter, we report on the total energy calculations for all 20  $\text{A}^{\text{I}}\text{B}^{\text{III}}$  ( $\text{A}^{\text{I}}$ : Li to Cs;  $\text{B}^{\text{III}}$ : Al to Tl) compounds with the WIEN2k package [23], on the estimation of their formation energies  $\Delta E^{\circ}_{\text{AB,f,0GPa,0K}}$  (kJ/mole) and on the estimation of the stabilizing pressure (GPa) for obtaining them in the DAC cell. In addition, we report also on high pressure in situ investigations up to 30 GPa with the DAC technique on the five thallides, such as LiTI, NaTI, KTI, RbTI, and CsTI.

## 2 Apparatus and Experimental Techniques

The apparatus and experimental techniques for studying the thallides LiTI, NaTI, KTI, RbTI, and CsTI in DAC technique are presented. The lithium, sodium, and potassium thallides were prepared at ambient pressure in a water-cooled copper boat by inductive heating of an equiatomic mixture of the constituent elements under argon. The rubidium and cesium  $\text{ATl}$  samples were synthesized by heating their equiatomic mixtures with thallium for 1 h at 500°C in corundum crucibles, which were placed in copper-sealed iron containers. In a DAC of Mao-Bell type, HP experiments were performed up to 30 GPa. Calibration of pressure was performed by adding 20% silver powder to the samples. With a  $\text{CO}_2$  laser system, the DAC could be heated in situ from both sides. Samples of RbTI and CsTI have been annealed for 2 h to about 100°C after HP treatment. By the Rietveld method, structural data were obtained. From literature, heat of formation data have been obtained for LiIn and for LiTI, at both 300 and 800 K.

The thallides LiTI, NaTI, and KTI were prepared at ambient pressure in a water-cooled copper boat by inductive heating of equiatomic mixtures with thallium under argon. Starting materials were lithium ingots (Alfa, nominal purity 99.9%), sodium and potassium metals (Koch-Light, 99.97%), and high-purity thallium (Johnson-Matthey, 99.997%). All manipulations were performed in a glove-box with high-purity argon. The reguli were cooled after each melting experiment, turned, and then molten several times again. Before last melting, the cold reguli were weighed back to control evaporation losses. After starting with alkali metal

excess, the required amount of thallium was added, followed by several melting procedures. Due to the high vapor pressure of rubidium and cesium, samples of 1:1 composition with thallium were heated 1 h at 500°C in a corundum crucible, which was placed in copper-sealed iron container. At ambient pressure, these samples have been annealed for 2 h to about 100°C. From such samples, X-ray Guinier diffractograms (MoK $\alpha_1$  radiation, quartz monochromator, 6–36° 2-theta, increment 0.04°, 20 s counting time per increment) were prepared for LiTl, NaTl, and KTl with isolated Tl<sub>6</sub>-octahedra [22], Rb<sub>8</sub>Tl<sub>11</sub> [24] +3 Rb and CsTl with isolated Tl<sub>6</sub>-octahedra [25].

In a piston-cylinder DAC of Mao-Bell type [26] (beveled 16-sided diamonds, culet: 300  $\mu\text{m}$ , T301 hardened stainless steel gasket, thickness: 80  $\mu\text{m}$ , hole: 130  $\mu\text{m}$ ), HP experiments were performed. No pressure-transmitting medium was applied. Calibration of pressure was performed by mixing 20% silver powder (5–8  $\mu\text{m}$ ; Johnson-Matthey Corp., #00785) to the samples. Specific volumes  $V/V_0$  of silver are tabulated as a function of pressure up to 90 GPa [27]. HP diffractograms were recorded either with AgK $\alpha$  radiation ( $\lambda = 0.5609$  Å, Pd-filter) or with MoK $\alpha$  radiation ( $\lambda = 0.7107$  Å, Zr-filter) in the theta range 3–13° (increment: 0.03°, typical counting time per increment: 600 s) with a collimator of 110  $\mu\text{m}$  diameter. With a double-sided CO<sub>2</sub> laser system, both diamonds of the DAC could be heated. Two laser beams come to both sides of the diamond anvil and improve the temperature distribution. By the Rietveld method [28], structural data were obtained from the smoothed diffractograms, fixing the zero point of the diffractometer.

Formation enthalpies for  $A^I B^{III}$  compounds  $\Delta H_{AB,f}$  which could be related to their stability are only known in a very few cases. Due to the experimental difficulties with these highly air- and moisture-sensitive  $A^I B^{III}$  compounds, such thermochemical data are mostly affected with very large uncertainties. A precise experimental procedure to obtain formation enthalpies  $\Delta H_{AB,f, 800\text{K}}$  for LiIn with the NaTl- and for LiTl with the  $\beta$ -brass-type structure has been applied by Predel et al. [29]. In Predel's group, the Li-compounds as well as the pure components have been dissolved at 800 K in a calorimeter filled with liquid tin. For the compounds and their components, with samples of about 20 g 5–10 measurements, respectively, caloric experiments had been carried out [29]. The formation enthalpies  $\Delta H_{AB,f, 800\text{K}}$  were obtained from the difference of the solution enthalpies of the components and the solution enthalpy of the compound [29]. The Miedema approach [30] was also applied to estimate enthalpies of formation  $\Delta H_{AB,f, 300}$  for LiIn and LiTl [29].

### 3 Computational Methods

The computational methods are presented. Total energy  $E^0$  calculations have been performed within the framework of DFT using the full-potential linearized augmented plane wave (LAPW) method embodied in the WIEN2k package. With the generalized

gradient approximation (GGA), the exchange and correlation effects were treated using the functional of Wu and Cohen. Following a series of trials varying the  $R_{\text{mt}}^*K_{\text{max}}$  values between 7 and 11, a value of 9 was used. The maximal G in charge density Fourier expansion was 14. The total energies of the binary  $A^I B^{\text{III}}$  compounds,  $E_{\text{AB}}^{\circ}$  and those of the constituents  $A^I$  and  $B^{\text{III}}$ ,  $E_{\text{A}}^{\circ}$  and  $E_{\text{B}}^{\circ}$ , were calculated for different volumes and fitting these data to Murnaghan's equation of state. After correction of the energies of formation  $\Delta E_{\text{AB,f}}^{\circ}$  for overbonding, 6 of the 20  $A^I B^{\text{III}}$  compounds have negative energies of formation and are therefore stable at zero pressure and temperature. From these fits, the equilibrium volumina and pressures were calculated, and, furthermore, the energies of formation at zero pressure and temperature via  $\Delta E_{\text{AB,f}}^{\circ} = E_{\text{AB}}^{\circ} - E_{\text{A}}^{\circ} - E_{\text{B}}^{\circ}$  and the pressures needed for stabilizing the NaTl-type phases up to 30 GPa have been estimated.

Total energy calculations were performed within the framework of the DFT using the full-potential LAPW method embodied in the WIEN2k package [23]. With the GGA, the exchange and correlation effects were treated using the functional of Wu and Cohen [31]. During the whole calculations, the following muffin tin radii were used with constant values (a.u.): Li 2.1, Na 2.3, K 2.4, Rb 2.5, Cs 2.6; Al 2.3, Ga 2.3, In 2.4, and Tl 2.5. Total energy calculations  $E^{\circ}$  for the  $A^I$  metals (Li to Cs) were performed with the body-centered cubic structures (I–3 m). For Al, the face-centered cubic structure (Fm–3m), for Ga and In the tetragonal body-centered structure (I4/mmm), and for Tl the hexagonal-closed packed structure (P6<sub>3</sub>/mmc) were used. The face-centered cubic structure (Fd–3m) was used for the  $A^I B^{\text{III}}$  compounds with the NaTl-type structure, the cubic primitive structure (Pm–3m) for the  $\beta$ -brass-type structure, and the body-centered tetragonal (I4<sub>1</sub>/amd) and the tetragonal primitive (P4/mmm) structure for the two distorted structures. Lattice parameters were taken from “Pearson's Handbook of Crystallographic Data for Intermetallic Phases” [32, 33]. For energy calculations the tetragonal distorted NaTl-type structure (I4<sub>1</sub>/amd), and for the CuAu-type structure (P4/mmm) lattice parameters were obtained by Rietveld analysis of diffractograms taken in our laboratory.

The total energies  $E_{\text{AB}}^{\circ}$ ,  $E_{\text{A}}^{\circ}$ , and  $E_{\text{B}}^{\circ}$  have been calculated for several volumes (e.g., typical changes (%): +20, +10, 0, –10, –20, –30, –40) and the volume–energy data were fitted to Murnaghan's equation of state [34]. From this fit, the equilibrium volume and pressure and the bulk moduli  $B_0$  (GPa) have been obtained. For a compound  $A^I B^{\text{III}}$ , the total enthalpy  $H^{\circ}$  is defined as  $H^{\circ} = E^{\circ} + pV$  ( $p$ : pressure,  $V$ : volume). Thus, at zero pressure it is  $H^{\circ} = E^{\circ}$ .  $E_{\text{AB}}^{\circ}$  is ground state–binding energy of the compound AB for one molecule. This value is derived from the total energy  $E_{\text{AB}}^{\circ}$ ,  $E_{\text{A}}^{\circ}$ , and  $E_{\text{B}}^{\circ}$ :  $E_{\text{AB,f}}^{\circ} = E_{\text{AB}}^{\circ} - E_{\text{A}}^{\circ} - E_{\text{B}}^{\circ}$ . At zero temperature and pressure with  $\Delta G_{\text{AB,f}}^{\circ} = \Delta H_{\text{AB,f}}^{\circ} + T \cdot \Delta S_{\text{AB,f}}^{\circ}$  the entropy term  $T \cdot \Delta S_{\text{AB,f}}^{\circ}$  is zero; therefore, the free enthalpy of formation  $\Delta G_{\text{AB,f}}^{\circ}$ , the enthalpy of formation  $\Delta H_{\text{AB,f}}^{\circ}$ , and the energy of formation  $\Delta E_{\text{AB,f}}^{\circ}$  are equal:  $\Delta G_{\text{AB,f}}^{\circ} = \Delta H_{\text{AB,f}}^{\circ} = E_{\text{AB,f}}^{\circ}$ . For the  $A^I B^{\text{III}}$  compounds, the heats of formation  $\Delta H_{\text{AB,f}}^{\circ}$  at increasing pressures (0, 5, 10, 15, 20, 25, 30 GPa) were interpolated from the eosfit files of the WIEN2k package [23], which were fitted by the Murnaghan equation [34] for the energy–volume data of  $E_{\text{AB}}$ ,  $E_{\text{A}}$ , and  $E_{\text{B}}$ , respectively. For Li to Cs, Al, Tl, NaTl-type, and  $\beta$ -brass-type

structure, 4,000 k points (leading to 120 k points in the irreducible part of the Brillouin zone) were used. For Ga and In, the analogous values were 4,000/188 and 2,000/159. The maximal  $l$  value for partial waves inside the atomic spheres was 10, and the maximal  $G$  (magnitude of the largest vector) in charge density Fourier expansion was 14. The total energy  $E^o$  calculations have been performed with  $R_{mt}^* K_{max}$  values of 9 with  $G_{max} = 14$ . With increasing of  $R_{mt}^* K_{max}$  from 7 to 11, such calculations lead to more negative  $E^o$  values for the  $A^I B^{III}$  compounds.

However, the total energy differences between the NaTl- and the  $\beta$ -brass-type structure  $\Delta E^o_{NaTl-\beta-brass}$  are not strongly affected by increasing  $R_{mt}^* K_{max}$ , e.g., for KIn the following energy differences were obtained with  $R_{mt}^* K_{max} = 7$ :  $-30.0$ , with 8:  $-29.3$ , with 9:  $-29.3$ , with 10:  $-29.6$ , and with 11:  $-29.6$  (in mRyd). Although KIn is unstable at zero pressure and temperature, the calculated energies of formation  $\Delta E^o_{AB,f}$ , e.g., for KIn are negative and increase slightly with increasing  $R_{mt}^* K_{max}$ , e.g., for  $R_{mt}^* K_{max} = 7$ ,  $\Delta E^o_{AB,f}$  is  $-10.4$ , for 8:  $-11.3$ , for 9:  $-11.8$ , for 10:  $-12.0$ , for 11:  $-11.9$ , for 12:  $-12.0$  (in mRyd). Also the calculated energies of formation  $\Delta E^o_{AB,f}$ , for NaGa, KTl, RbIn, RbTl, CsTl become negative by WIEN2k calculation, implying that these compounds would be stable at zero pressure and temperature. This would lead to 12 stable  $A^I B^{III}$  compounds at zero pressure and energy. This is contradictory to the experimental facts that only six of them are stable at ambient conditions. Therefore, the energies of formation  $\Delta E^o_{AB,f}$ , calculated with  $R_{mt}^* K_{max} = 9$  and  $G_{max} = 14$  have to be corrected for overbonding.

For LiIn and LiTl, the overbonding correction was fitted via the tabulated enthalpies of formation  $\Delta H_{AB,f,800}$ , measured by solution calorimetry and also calculated by the Miedema approach [29, 30]. For LiIn, the experimental energies of formation are  $\Delta H_{LiIn,f,800} = -49$  kJ/mole (solution calorimetry) [29] and  $\Delta H_{LiIn,f,300} = -46$  kJ/mol (Miedema approach) [29, 30]. The analogous energies of formation for LiTl are  $\Delta H_{LiTl,f,800} = -40$  kJ/mole (solution calorimetry) [29] and  $\Delta H_{LiIn,f,300} = -55$  kJ/mol (Miedema approach) [29, 30].

The applied overbonding corrections for the 20  $A^I B^{III}$  compounds are shown in Fig. 1. They increase from LiAl with  $-1.0$  to CsTl with  $-22.0$  mRyd.

For LiTl ( $\beta$ -brass-type structure) and for LiIn and KTl (NaTl-type structure), the overbinding correction for the energies of formation  $\Delta E^o_{AB,f}$  was also determined with the local spin density approximation (LSDA) by Perdew [35] and with the GGA by Perdew, Burke, and Ernzerhof ("Standard PBE") [36]. The overbinding corrections for LiIn, LiTl, and KTl obtained with GGA by Wu and Cohen [31] are 20% lower than those obtained with LSDA [35], but 15% higher than those obtained with "Standard PBE" GGA [36].

## 4 Crystal Structures

The crystal structures that were observed during the HP experiments with the DAC are presented here. The cubic NaTl- and the cubic  $\beta$ -brass-type structure are compared with each other. Two tetragonal distortions of both cubic phases are

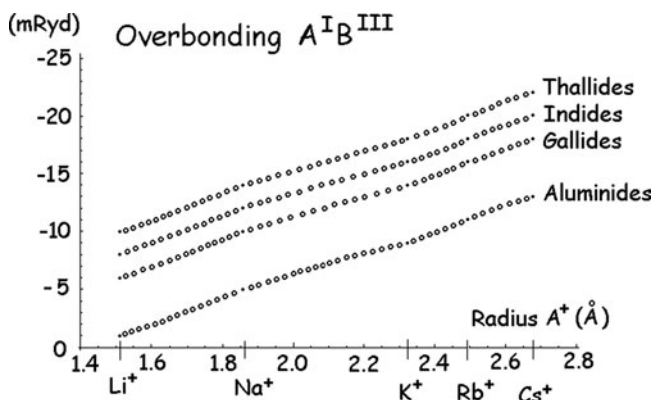


**Fig. 1** Overbonding correction (mRyd) for  $A^I$  aluminides, gallides, indides, and thallides as function of the radius  $A^+$  (Å) with  $Li^+$  1.509,  $Na^+$  1.858,  $K^+$  2.323,  $Rb^+$  2.493,  $Cs^+$  2.678

also discussed here. Both are obtained by a symmetry reduction in a group–subgroup relation “translationgleich” of index t3 from the cubic phases. The tetragonal distortion derived from the NaTl-type structure (Fd-3m) was found in 2002 by Ehrenberg et al. as low temperature phase of LiIn ( $I_4/amd$ ). The AuCu-type structure is the tetragonal distortion of the  $\beta$ -brass-type structure (P4/mmm) and was obtained in this investigation as HP phase of LiTl. In the 1930s of the last century, Zintl had observed this structure for LiBi and NaBi at ambient pressure.

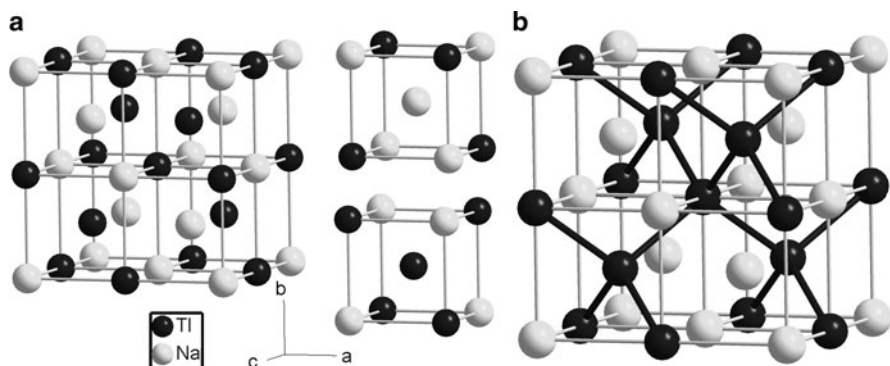
#### 4.1 NaTl-Type Structure

Figure 2 shows two views on the NaTl-type crystal structure, Pearson symbol cF16, space group Fd-3m with 8 f.u. per unit-cell. The face-centered cubic unit-cell of NaTl-type structure consists of eight small cubes, alternatively centered either with  $A^I$  or  $B^{III}$  atoms (Fig. 2a). Each of these centered sites has eight neighbors: four like and four unlike. The  $A^I$  and the  $B^{III}$  atoms lie on diamond sublattices, which are separated by a quarter of the body diagonal of the unit-cell. In the Zintl concept [1–6] of  $Na^+Tl^-$ , negatively charged  $Tl^-$  ion forms four equidistant and equiangled covalent bonds as they are observed in the diamond structure of tetrel elements  $C_{dia}$ , Si, Ge,  $\alpha$ -Sn at ambient pressure (Fig. 2b). Up to now, six binary  $A^IB^{III}$  compounds crystallize in the NaTl-type structure. Zintl had characterized five compounds such as LiAl [1], LiGa [14], LiIn [14], NaIn [13], and NaTl [8] at ambient pressure, and one novel was observed by Evers and Oehlinger KTI at HP of 2 GPa [21].

#### 4.2 $\beta$ -Brass-Type Structure

Figure 3 shows a view on the  $\beta$ -brass-type crystal structure, Pearson symbol cP2, and space group Pm-3m with two f.u. per unit-cell. The cubes in the  $\beta$ -brass-type





**Fig. 2** View on the NaTl-type crystal structure, Pearson symbol cF16, space group Fd-3m. (a) The face-centered cubic arrangement of eight smaller cubes alternatively centered either with Tl or Na atoms. (b) In the Zintl concept of  $Na^+Tl^-$ , one electron is transferred from the electropositive Na atoms to the electronegative Tl atoms. By this electron transfer, the  $Tl^-$  ion forms four covalent bonds, as they are observed in the diamond structure of tetrel elements C, Si, Ge, and  $\alpha$ -Sn

structure are either centered with  $A^I$  atoms or, after a shift of the origin with halve of the body diagonal, with  $B^{III}$  atoms. In the NaTl-type and in the  $\beta$ -brass alloy structure, each site has eight near neighbors in interpenetrating cubes, however, with different ordering. In contrast to the NaTl-type, in the  $\beta$ -brass-type structure there are eight equidistant  $A^I B^{III}$  contacts for every site. At ambient pressure, the  $A^I B^{III}$  compound LiTl crystallizes due to Zintl's investigation [14] with this structure. Schwarz et al. [20] prepared at HP LiIn with the  $\beta$ -brass-type structure. Since the lattice parameter of LiIn obtained at HP is approximately halved in comparison to the NaTl-type structure, eight cubic unit-cells of the  $\beta$ -brass-type structure have nearly the same volume as one of the normal pressure phase (Fig. 3).

### 4.3 Tetragonal Distorted NaTl-Type Structure

Due to low temperature investigations of Ehrenberg et al. [19], LiIn transforms at 170 K at ambient pressure into a tetragonal distorted NaTl-type structure, Pearson symbol tI8, space group  $I4_1/amd$  with four f.u. per unit-cell. The symmetry is reduced in a reversible group-subgroup "translationengleich" transition of index 3 (t3). The tetragonal distortion is with 0.5% [19] very small. The first Li-In coordination shells are only slightly distorted. Distances are not affected, but the ideal tetrahedral angle of  $109.47^\circ$  splits into those with  $109.20^\circ$  and  $109.61^\circ$  [19]. Neglecting this small distortion, the low temperature structure of LiIn (Fig. 3) in this distorted NaTl-type structure contains alternatively centered interpenetrating cubes that have four like and four unlike neighbors. Figure 4 shows a view on the low temperature structure of LiIn.

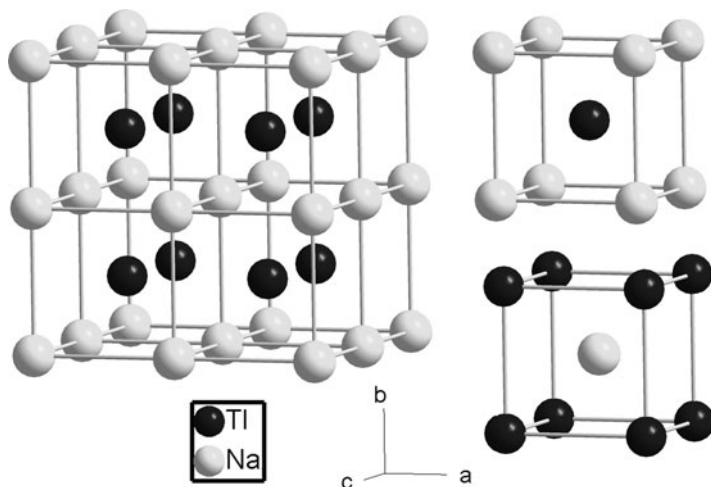


**Fig. 3** View on eight unit-cells of the  $\beta$ -brass alloy crystal structure, Pearson symbol cP2, space group Pm-3m. The unit-cells are either centered with A atoms or after a shift of halve of the body diagonal with B<sup>III</sup> atoms. Every site has eight A<sup>I</sup>-B<sup>III</sup> contacts equidistant and equiangular

#### 4.4 AuCu-Type Structure

The AuCu-type structure, Pearson symbol tP4, space group P4/mmm with two f.u. per unit-cell ( $z = 2$ ), can be considered as a tetragonal distortion of the  $\beta$ -brass alloy structure (CsCl-type structure) ( $z = 1$ ). The transformation of the  $\beta$ -brass-type structure (Pm-3m) into the tetragonal distorted structure with  $z = 1$  (P4/mmm) is also a symmetry reduction “translationgleich” of index 3 (t3). Zintl and coworkers determined the tetragonal distorted  $\beta$ -brass alloy structure with  $z = 1$  for LiBi [37] and for NaBi [38]. In Sect. 5.4, the structural data for LiBi and NaBi will be transformed into those for the AuCu-type structure ( $z = 2$ ) to compare it with the high pressure phase determined here for LiTl. In Fig. 5, the AuCu-type structure and the tetragonal distorted  $\beta$ -brass-type structure are shown.

The normal pressure phases of KTl [22] and CsTl [25] with isolated  $\text{Ti}_6^-$  octahedral, which are easily transformed at HP, are not considered here.

## 5 Results and Discussion

The results of the WIEN2k calculations are presented for aluminides, gallides, indides, and thallides. In addition, experimental results of in situ HP investigations in the DAC on thallides are presented here. The WIEN2k calculations show that for three A<sup>I</sup>B<sup>III</sup> compounds with small radius ratio ( $r_A:r_B$  from 1.0 to 1.1) LiAl, LiGa, and NaTl, the NaTl-type structure could be transformed into the  $\beta$ -brass-type structure in the pressure range up to 40 GPa. These compounds simulate the

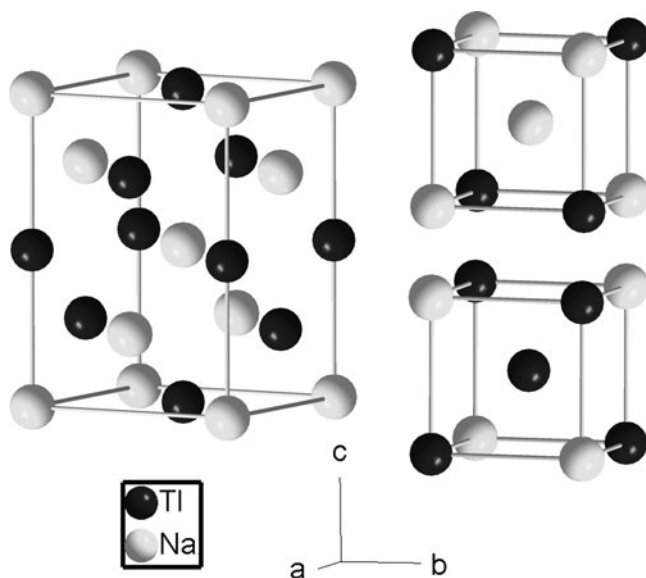


**Fig. 4** View on the low temperature phase of LiIn with the tetragonal distorted NaTl-type crystal structure, Pearson symbol tI8, space group  $I4_1/amd$ . The tetragonal distortion is with 0.5% small. The body-centered cubic arrangement of this structure contains interpenetrating cubes alternatively centered either with  $A^I$  or with  $B^{III}$  atoms with four like and four unlike neighbors. The transition of  $\alpha$ -Sn ( $Fd\bar{3}m$ ) into  $\beta$ -Sn ( $I4_1/amd$ ) at  $15^\circ$  follows the same route of symmetry reduction, as has been observed for the In atoms in LiIn. The transition in Sn is also “translationengleich” of index 3, but the tetragonal distortion in  $\beta$ -Sn is much stronger than in LiIn. Due to the strong compression of the  $c$ -lattice parameter in  $\beta$ -Sn, the coordination of the Sn atoms is increased from four to six with a density increase of about 20%, which is about 40 times stronger than in LiIn

behavior of LiTl at ambient pressure. For higher  $r_A:r_B$  ratios, the NaTl-type structure is more stable than the  $\beta$ -brass-type structure. In a DAC diffractograms of LiTl, NaTl, KTl, RbTl, and CsTl were obtained and then analyzed with the Rietveld technique. For 19  $A^I B^{III}$  compounds with the NaTl-type structure, the lattice parameters have been determined and the near-neighbor diagram for these phases has been derived. The near-neighbor diagram, introduced by Pearson in 1968, is used to get information on the bonding characteristics for intermetallic compounds. For the NaTl-type structure, it is now extended from radius ratio  $r_A:r_B$  of 1.15 for five at that time actual phases known by Pearson to now 19 phases with such a ratio up to 1.90.

### 5.1 Aluminides LiAl, NaAl, KAl, RbAl, and CsAl

The binary phase diagrams of the 1:1 alkali aluminides show at 1 bar two different types of phase diagrams [39]. The congruent melting of LiAl at  $700^\circ\text{C}$  allows an easy preparation from a melt with 1:1 composition. The phase diagrams

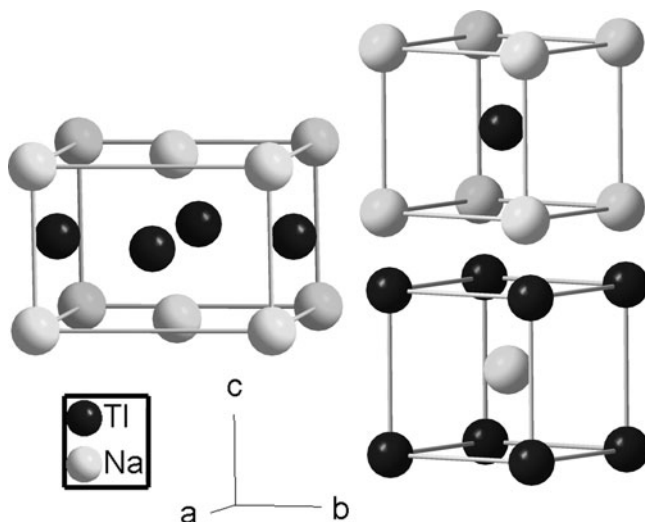


**Fig. 5** View on AuCu alloy structure, Pearson symbol tP4, space group P4/mmm. This structure can be considered as tetragonal distorted  $\beta$ -brass alloy structure. The AuCu structure contains two f.u. The tetragonal distortion is stronger than in the low temperature phase LiIn. In the AuCu-type structure, there are tetragonal distorted interpenetrating cubes, and are either centered with  $A^I$  or  $B^{III}$  atoms. Each of these interpenetrating cubes contains only one formula unit AuCu and can be considered as an own structure, Pearson symbol tP2, space group P4/mmm

Na-Al, K-Al, Rb-Al, and Cs-Al show that these elements are practically immiscible in the liquid state near the melting point of Al at 660°C [39]. Therefore, the compounds NaAl, KAl, RbAl, and CsAl could not be prepared up to now from a melt at 1 bar.

In Table 1, the calculated total energy  $E^o$  (Ryd), the volume  $V_o$  ( $\text{\AA}^3$ ), both for one f.u., and the bulk moduli  $B_o$  (GPa) for the aluminides LiAl, NaAl, KAl, RbAl, and CsAl with the NaTl- and the  $\beta$ -brass-type structure at zero pressure and temperature are summarized.

For the stable compound LiAl, the lattice parameter for the NaTl-type structure ( $z = 8$ )  $a_{0K,0GPa}$  is calculated via the cubic root of  $8 \cdot V_o$ . With  $V_o = 31.71 \text{ \AA}^3$  (Table 1),  $a_{0K,0GPa} = 6.33 \text{ \AA}$  is calculated. The tabulated lattice parameters [32, 33] for LiAl are  $a_{300K,1bar}$ : 6.3667, 6.3703, 6.3757, in  $\text{\AA}$ , with an average value of  $a_{300K,average} = 6.371 \text{ \AA}$ , leading to a unit-cell volume of  $V_{average300K} = 258.6 \text{ \AA}^3$ . In order to compare both lattice parameters, one has to correct the experimental lattice parameter of LiAl for thermal expansion.

During this investigation, the lattice parameters of LiIn with the NaTl-type structure have been determined from Guinier diffractograms with  $\text{CuK}\alpha_1$  radiation at 300 and 200 K and for the tetragonal distorted NaTl-type structure at 100, 50, 30, and 10 K (Table 7). For LiIn with a cubic unit-cell volume at 300 K of  $313.7 \text{ \AA}^3$ , there is on cooling to 10 K a volume decrease of  $\Delta V = -5.63 \text{ \AA}^3$  for the tetragonal phase. For LiAl with a volume of  $258.6 \text{ \AA}^3$  at 300 K, assuming

**Table 1** Calculated total energy  $E^\circ$  (Ryd), volume  $V_o(\text{\AA}^3)$  for one f.u., and bulk moduli  $B_o$  (GPa) of aluminides LiAl, NaAl, KAl, RbAl, and CsAl with the NaTl- and the  $\beta$ -brass-type structure at zero pressure and temperature

	NaTl-type structure			$\beta$ -Brass-type structure		
	$E^\circ(\text{Ryd})$	$V_o(\text{\AA}^3)$	$B_o(\text{GPa})$	$E^\circ(\text{Ryd})$	$V_o(\text{\AA}^3)$	$B_o(\text{GPa})$
LiAl	-500.23568	31.71	46	-500.22393	30.66	42
NaAl	-809.73778	41.90	32	-809.70616	46.19	25
KAl	-1,688.82481	54.44	22	-1,688.78208	66.12	14
RbAl	-6,447.04091	60.49	20	-6,447.00136	74.48	12
CsAl	-16,064.10790	65.27	22	-16,064.06805	75.66	15

proportionality of thermal expansion between LiIn and LiAl, a decrease of  $\Delta V = -4.6 \text{ \AA}^3$  is calculated (volume of  $254.0 \text{ \AA}^3$  at 10 K, 1 bar). The experimental lattice parameter of LiAl ( $a_{300\text{K}, 1\text{bar}} = 6.371 \text{ \AA}$ ) is then decreased to  $a_{10\text{K}, 1\text{bar}} = 6.33 \text{ \AA}$ , which is now in total agreement with the calculated lattice parameter (WIEN2k) of  $a_{0\text{K}, 0\text{bar}} = 6.33 \text{ \AA}$ . With the local density approach (LDA), Christensen calculated in 1985 a  $a_{0\text{K}, 0\text{bar}} = 6.328 \text{ \AA}$  for LiAl [18].

Inspection of Table 1 shows that LiAl with the NaTl-type and the  $\beta$ -brass-type structure have the highest bulk moduli  $B_o$  (46, 42, respectively) of all the 1:1 alkali aluminides. LiAl is therefore the hardest material of these aluminides. Table 1 indicates also that the bulk moduli of the phase with the  $\beta$ -brass-type structure have lower  $B_o$  values than those for NaTl-type structure and are, therefore, more ductile. Thus, the phases with the  $\beta$ -brass type seem to have more alloy character than those with the NaTl-type structure with partly covalent bonding in the  $\text{TI}^-$  net. Christensen [18] calculated in 1985 the bulk modulus of LiAl with the NaTl-type structure to 45.0 GPa at the theoretical equilibrium volume. Interestingly, the bulk moduli  $B_o$  of CsAl (22, 15 GPa) are higher than those of RbAl (20, 12 GPa) (Table 1).

The differences in energy  $\Delta E^\circ$  and volume  $\Delta V_o$  between the phases with NaTl- and  $\beta$ -brass-type structure (Table 1) are strongly dependent on the size of the alkali metals. In Fig. 6, the energy difference  $\Delta E$  (Ryd) between the NaTl- and the  $\beta$ -brass type as function of the radii ( $\text{\AA}$ ) from Li to Cs is shown; in Fig. 7, the volume difference  $\Delta V$  (a.u.<sup>3</sup>) between both structures is plotted.

Interestingly, the  $\beta$ -brass-type phase of LiAl is the only phase of the 1:1 alkali aluminides which is lower in volume  $V_o$  ( $30.66 \text{ \AA}^3$ , Table 1,  $206.93 \text{ a.u.}^3$ , with  $1 \text{ a.u.} = 0.529177 \text{ \AA}$ ) than the NaTl-type structure ( $31.71 \text{ \AA}^3$ , Table 1,  $214.01 \text{ a.u.}^3$ ), although the energy  $E^\circ$  of the first ( $-5000.22393 \text{ Ryd}$ , Table 1) is  $-11.76 \text{ mRyd}$  lower than that of the second ( $-500.23568 \text{ Ryd}$ , Table 1). Christensen calculated this energy difference  $-12.6 \text{ mRyd}$  [18]. However, as can be seen in Fig. 7, the energy difference between the NaTl- and the  $\beta$ -brass type in the series of aluminides is the lowest for LiAl. Therefore, applying high pressure on LiAl one could transform the NaTl-type structure. In Fig. 8, the total energies  $E^\circ$  (Ryd) and the volumes  $V$  (a.u.<sup>3</sup>) for LiAl with the NaTl- and the  $\beta$ -brass type are plotted as function of the unit-cell volume.

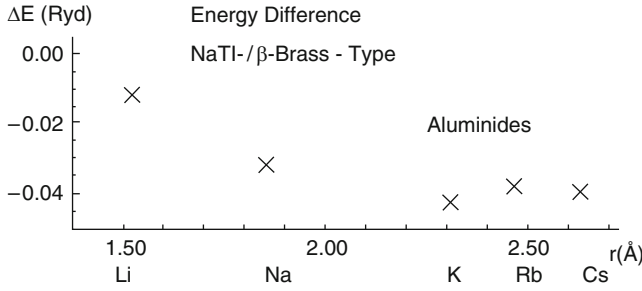


**Fig. 6** Energy difference  $\Delta E^\circ$  (Ryd) between the NaTi- and the  $\beta$ -brass-type structures of LiAl, NaAl, KAl, RbAl, and CsAl as function of the radii (Å) for the alkali metals (CN 8)

At about 155 a.u.<sup>3</sup>, the total energies  $E^\circ$  for both phases are equal, thus allowing coexistence of both phases. From the fit of the volume–energy data with Murnaghan’s equation of state [34], a pressure of 25 GPa can be estimated for the transformation of the NaTi- into the  $\beta$ -brass-type structure of LiAl.

For NaAl, the difference in energy is too high that a HP transformation in the range up to 30 GPa into the  $\beta$ -brass-type structure seems to be successful. As it has been already mentioned in Sect. 3, the energy of formation  $\Delta E_{AB,f}^\circ$  at zero temperature and pressure can be calculated from the total energies  $E_{AB}^\circ$ ,  $E_A^\circ$ , and  $E_B^\circ$  with the  $\Delta E_{AB,f}^\circ = E_{AB}^\circ - E_A^\circ - E_B^\circ$ . In Table 2, the energies of formation for NaAl  $\Delta E_{f,NaAl}^\circ$  (Ryd) with increasing pressure are summarized, without applying an overbonding correction. From inspection of Table 2, it is evident that the reaction  $\text{Na(s)} + \text{Al(s)} \rightarrow \text{NaAl(s)}$  at zero temperature and pressure leads to a positive energy of formation  $\Delta E_{NaAl,f}^\circ = +19.04$  mRyd, which converts into  $\Delta E_{NaAl,f}^\circ = +25$  kJ/mole. After correction for overbonding (+5.0 mRyd for NaAl),  $\Delta E_{NaAl,f,corr}^\circ = +19.04 + 5.0 = +24.04$  mRyd, which converts into  $\Delta E_{NaAl,f,corr}^\circ = +32$  kJ/mole. The reaction to form NaAl from the constituent metals is therefore endergonic at zero pressure and temperature. However, with increasing pressure the positive  $E_{NaAl,f}^\circ$  values decrease (Table 2) until at 25 GPa the reaction is exergonic with  $\Delta E_{NaAl,f}^\circ = -5.13 + 5.0 = -0.13$  mRyd (Table 2), after overbonding correction. The reason for the decrease of the positive values of  $\Delta E_{NaAl,f}^\circ$  in the pressure range up to 25 GPa is the stronger decrease of  $E_{Na}^\circ$  in comparison to  $E_{Al}^\circ$  and to  $E_{NaAl}^\circ$ .

At 1 bar, NaAl cannot be prepared from the liquid elements, because sodium and aluminum are practically immiscible at the melting point of Al [39]. Therefore, with a synthesis in DAC with double-sided laser heating at about 25 GPa, there could be a chance to synthesize NaAl with the NaTi-type structure.

The estimated energies of formation  $\Delta E_{AB,f,0K,0GPa}^\circ$  of NaTi-type phases LiAl to CsAl and the estimated pressure (GPa) for stabilizing the NaTi-type structure in NaAl to CsAl are summarized in Table 3.

For 1:1 alkali aluminides, LiAl is the only stable phase with the NaTi-type structure at 1 bar. The estimated energy of formation (WIEN2k) at zero pressure and temperature is  $\Delta E_{LiAl,f,0K,0GPa}^\circ -33$  kJ/mole. With increasing metal radius from Na to Cs, the

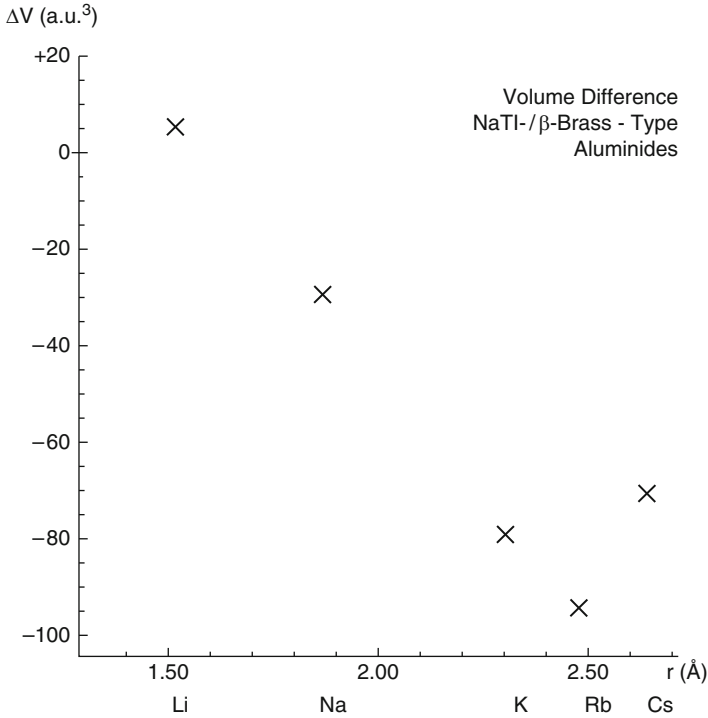


**Fig. 7** Volume difference  $\Delta V_o$  (a.u.<sup>3</sup>) between the NaTl- and the  $\beta$ -brass-type structures of LiAl, NaAl, KAl, RbAl, and CsAl as function of the radii (Å) for the alkali metals (CN 8)

endergonic formation energies increase drastically (NaAl +32, KAl +70, RbAl +90, CsAl +100 kJ/mole; Table 3). The estimated stabilization pressure for the alkali aluminides with the NaTl-type structure from NaAl to CsAl lies in the range between 25 and 30 GPa (Table 3).

## 5.2 Gallides *LiGa*, *NaGa*, *KGa*, *RbGa*, and *CsGa*

The binary phase diagrams of the 1:1 alkali gallides show at 1 bar nearly the analogous behavior as the 1:1 alkali aluminides. The congruent melting of LiGa at 730°C [39] allows only the preparation of this compound from a melt. The phase diagrams Na-Ga, K-Ga, Rb-Ga and Cs-Ga indicate that these elements are practically immiscible in the liquid state [39]. Therefore, the compounds NaGa, KGa, RbGa, and CsGa cannot be prepared up to now from a melt at 1 bar.

In Table 4, the calculated total energy  $E^o$  (Ryd), the volume  $V_o$  (Å<sup>3</sup>), both for one f.u., and the bulk moduli  $B_o$  (GPa) for the gallides LiGa, NaGa, KGa, RbGa, and

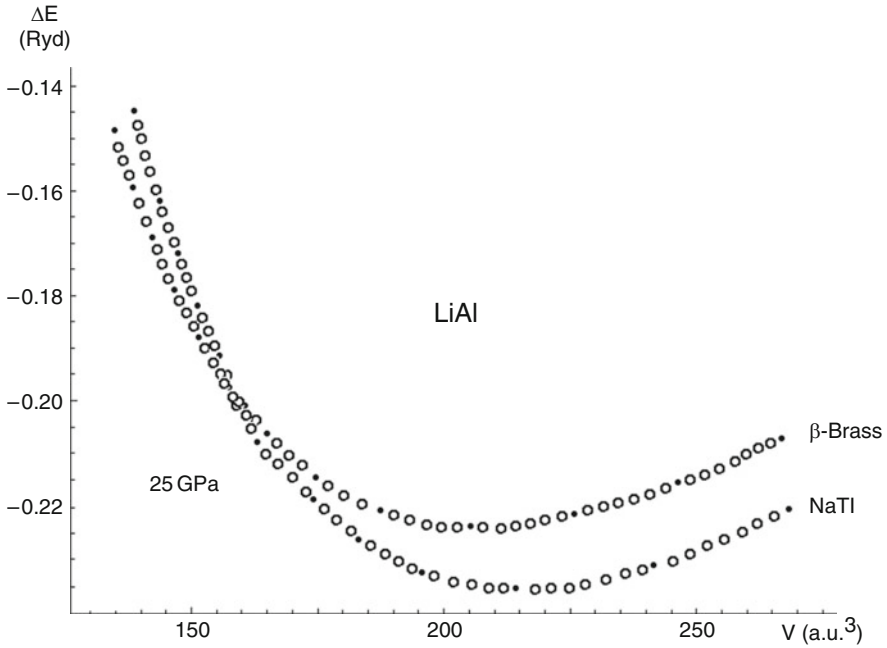


**Fig. 8** Total energy  $E^\circ$  (Ryd) curves for LiAl with the NaTl- and the  $\beta$ -brass-type as function of the unit-cell volume  $V$  (a.u.<sup>3</sup>). Below 155 a.u.<sup>3</sup> the NaTl-type structure of LiAl is the stable phase

**Table 2** Estimation of the energy of formation  $\Delta E^\circ_{f,NaAl}$  (Ryd) for NaAl with the NaTl-type structure as function of the pressure  $p$  (GPa) up to 40 GPa, not corrected for overbonding

$p$ (GPa)	Na(s) (Ryd)	Al(s) (Ryd)	NaAl(s) (Ryd)	$\Delta E^\circ_{f,NaAl,0K}$ (Ryd)
40	-324.42771	-485.20887	-809.65118	-0.01460
35	-324.43806	-485.21369	-809.66350	-0.01160
30	-324.44903	-485.21835	-809.67588	-0.00849
25	-324.46026	-485.22276	-809.68815	-0.00513
20	-324.47199	-485.22689	-809.70037	-0.00149
15	-324.48423	-485.23061	-809.71226	+0.00257
10	-324.49740	-485.23373	-809.72342	+0.00771
5	-324.51011	-485.23599	-809.73290	+0.01319
0	-324.51991	-485.23690	-809.73778	+0.01904

CsGa with the NaTl- and the  $\beta$ -brass-type structure at zero pressure and temperature are summarized.

The differences in energy  $\Delta E^\circ$  and volume  $\Delta V_o$  between the phases with NaTl- and  $\beta$ -brass-type structure (Table 4) are strongly size dependent. For LiGa, the difference in energy is  $\Delta E^\circ = -10.2$  mRyd and the difference in volume  $\Delta V_o = -0.26$  Å<sup>3</sup>, but for CsGa such values are  $-20.7$  mRyd and  $-12.15$  Å<sup>3</sup>, respectively. Christensen calculated for LiGa the energy difference between the NaTl- and the  $\beta$ -brass-type structure to  $-8.6$  mRyd [18].



**Table 3** Estimated energy of formation  $\Delta E^\circ_{f,AB,0GPa}$  (kJ/mole) for LiAl to CsAl, and estimated pressure (GPa) for NaTl phases stabilized in NaAl to CsAl

$A^I B^{III}$ phase with NaTl-type structure	LiAl	NaAl	KAl	RbAl	CsAl
$\Delta E^\circ_{f,AB,0GPa}$ (kJ/mole)	-33	+32	+70	+90	+100
Stabilization pressure (GPa)	0	25	30	30	30

Inspection of Table 4 shows that LiGa with the NaTl-type and the  $\beta$ -brass-type structure has the highest bulk moduli  $B_o$  (45, 41 GPa, respectively). LiGa is therefore the hardest material of these alkali gallides. Christensen calculated the bulk modulus  $B_o$  of LiGa to 43.3 GPa [18]. Table 4 shows also that the bulk moduli  $B_o$  of the phases with the  $\beta$ -brass type have lower values than those with NaTl-type structure. Therefore, the first are more ductile than the second. Interestingly, the bulk modulus  $B_o$  of CsGa with the NaTl-type structure (22 GPa) is higher than that of RbGa (19 GPa), although one would expect the opposite.

For the ambient pressure stable compound LiGa, the lattice parameter  $a_{0K,0GPa}$  for the NaTl-type structure ( $z = 8$ ) is calculated from the cubic root of  $8 \cdot V_o$ . With  $V_o = 29.45 \text{ \AA}^3$  (Table 1), one calculates  $a_{0K,0GPa} = 6.18 \text{ \AA}$ . The tabulated lattice parameters [32, 33] for LiGa are  $a_{300K,1bar}$ : 6.195, 6.22, 6.150, in  $\text{\AA}$ , with an average value of  $a_{300K,average} = 6.188 \text{ \AA}$ , leading to a unit-cell volume of  $V_{average,300K} = 236.95 \text{ \AA}^3$ . After correction for thermal expansion, the experimental lattice parameter of LiGa ( $a_{300K,1bar} = 6.188 \text{ \AA}$ ) is then decreased to  $a_{10K,1bar} = 6.15 \text{ \AA}$ , which is now in very good agreement with the calculated lattice parameter (WIEN2k) of  $a_{0K,0bar} = 6.18 \text{ \AA}$ . Christensen had calculated the lattice parameter of LiGa to  $a_{0K,0GPa} = 6.405 \text{ \AA}$  [18]. The large deviation of this calculated value (6.405  $\text{\AA}$ ) to the experimental one (6.195  $\text{\AA}$ ), Christensen commented that he had “Ga 3d treated as frozen states (causes overestimate of  $a_{theor}$ )” [18].

In Fig. 9, the total energies  $E^\circ$  (Ryd) and the volumes  $V$  (a.u.<sup>3</sup>) for LiGa with the NaTl- and the  $\beta$ -brass type are plotted as function of the unit-cell volume. At about 140 a.u.<sup>3</sup>, the total energy  $E^\circ$  curves touch each other. The phases of LiGa with the NaTl- and with the  $\beta$ -brass-type structure coexist in this case. With an energy difference of  $-10.2 \text{ mRyd}$  ( $= -13 \text{ kJ/mole}$ , Table 4), the transformation pressure is approximately 25 GPa. The difference in energy is for NaGa ( $-21.7 \text{ mRyd} = -28 \text{ kJ/mole}$ ; Table 4) too high that NaGa can be transformed up to 30 GPa into the  $\beta$ -brass-type structure.

The estimated energies of formation  $\Delta E^\circ_{f,AB,0K,0GPa}$  for LiGa to CsGa and the estimated pressure (GPa) for NaGa to CsGa stabilizing the NaTl-type structure are summarized in Table 5. For alkali gallides, LiGa is the only stable phase with the NaTl-type structure at 1 bar. The estimated energy of formation (WIEN2k) for LiGa at zero pressure and temperature is  $\Delta E^\circ_{f,LiAl,f,0K,0GPa} = -61 \text{ kJ/mole}$ . With increasing metal radius from Na to Cs, the endergonic formation energies increase drastically. The estimated stabilization pressure for the alkali gallides NaGa to CsGa with the NaTl-type structure lies in the range between 5 and 15 GPa (Table 5).

**Table 4** Calculated total energy  $E^\circ$ (Ryd), volume  $V_o(\text{\AA}^3)$  for one f.u., and bulk modulus  $B_o$ (GPa) of gallides LiGa, NaGa, KGa, RbGa, and CsGa with the NaTl- and the  $\beta$ -brass-type structure at zero pressure and temperature

	NaTl-type structure			$\beta$ -Brass-type structure		
	$E^\circ$ (Ryd)	$V_o(\text{\AA}^3)$	$B_o$ (GPa)	$E^\circ$ (Ryd)	$V_o(\text{\AA}^3)$	$B_o$ (GPa)
LiGa	−3,902.35348	29.45	45	−3,902.34327	29.71	41
NaGa	−4,211.85705	40.13	30	−4,211.83539	44.45	26
KGa	−5,090.94716	52.60	20	−5,090.91811	63.21	16
RbGa	−9,849.16447	59.05	19	−9,849.13731	70.36	14
CsGa	−19,466.23272	63.99	22	−19,466.21205	76.14	14

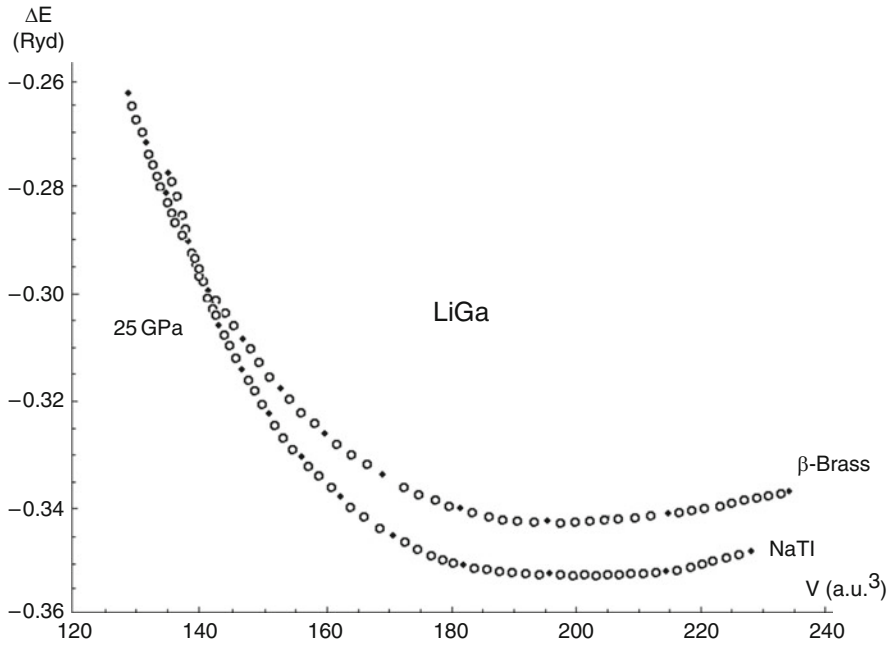


**Fig. 9** Total energy  $E^\circ$  (Ryd) curves for LiGa with the NaTl- and the  $\beta$ -brass-type as function of the unit-cell volume  $V$  (a.u.<sup>3</sup>). At 140 a.u.<sup>3</sup>, the total energy with about 25 GPa pressure, the total energy  $E^\circ$  curves touch each other. At this pressure, the NaTl- and the  $\beta$ -brass-type structure of LiGa are in equilibrium

### 5.3 Indides LiIn, NaIn, KIn, RbIn, and CsIn

The binary phase diagrams of the 1:1 alkali indides show at 1 bar different types of phase diagrams [39]. As observed for LiAl and LiGa, also LiIn melts congruently [632(5)°C]. For NaIn, less stable than LiIn, no dystectical, but peritectical melting at 345(4)°C is found. No compound KIn is stable in the K-In-system, but there is a miscibility gap near 1:1 composition. Such a behavior occurs also for the Rb-In and the Cs-In system.

**Table 5** Estimated energy of formation  $\Delta E^\circ_{f,AB,0K,0GPa}$  (kJ/mole) for LiGa to CsGa and estimated pressure (GPa) for NaTl-type phases stabilized in NaGa to CsGa

$A^I B^{III}$ phase with NaTl-type structure	LiGa	NaGa	KGa	RbGa	CsGa
$\Delta E^\circ_{f,AB,0K,0GPa}$ (kJ/mole)	-61	+2	+36	+64	+63
Stabilization pressure (GPa)	0	5	10	15	10

In Table 6, the calculated total energy  $E^\circ$  (Ryd), the volume  $V_o$  ( $\text{\AA}^3$ ), both for one f.u., and the bulk moduli  $B_o$  (GPa) for the indides LiIn, NaIn, KIn, RbIn, and CsIn with the NaTl- and the  $\beta$ -brass-type structure at zero pressure and temperature are summarized.

As it has been also observed for aluminides and gallides, for indides the differences in energy  $\Delta E^\circ$  and volume  $\Delta V_o$  between the phases with NaTl- and  $\beta$ -brass-type structure (Table 4) are strongly size dependent, having in mind that LiIn with  $\beta$ -brass-type structure – due to this investigation – is more stable than that with the NaTl-type phase ( $-1.1$  mRyd). Christensen, however, calculated in 1985 for LiIn the opposite that NaTl-type structure  $-1.3$  mRyd more stable than the  $\beta$ -brass-type structure [18]. Due to our results, LiIn with NaTl-type structure is then high temperature phase at 1 bar, the  $\beta$ -brass modification low temperature phase. With a volume  $V_o = 37.69 \text{ \AA}^3$ , the  $\beta$ -brass phase of LiIn has also a lower volume than the NaTl-type phase ( $39.46 \text{ \AA}^3$  with  $\Delta V_o = -1.77 \text{ \AA}^3 = -4.3\%$ ). However, for NaIn to CsIn the differences in energy and in volume between the NaTl- and the  $\beta$ -brass-type structure increase. For NaIn,  $\Delta E^\circ = -16.8$  mRyd and in volume  $\Delta V_o = -2.54 \text{ \AA}^3$ , but for CsIn these values are  $-26.1$  mRyd and  $-14.93 \text{ \AA}^3$ , respectively (Table 6). Christensen has calculated the energy difference between the NaTl- and  $\beta$ -brass-type structure for NaIn to  $-14.2$  mRyd [18].

Inspection of Table 6 shows that LiIn phases with the NaTl-type and the  $\beta$ -brass-type structure have the highest bulk moduli  $B_o$  (36, 35 GPa, respectively) and are therefore the hardest materials of these 1:1 alkali indides. NaIn has bulk moduli  $B_o$  (28, 25 GPa, respectively, for the NaTl- and the  $\beta$ -brass-type structure). Christensen calculated a bulk modulus  $B_o$  of 34.7 GPa for LiIn and for 31.1 GPa for NaIn with the NaTl-type structure [18]. Schwarz et al. derived experimentally the bulk moduli  $B_o$  of LiIn [39(5), 46(5) in GPa, respectively, for the NaTl- and the  $\beta$ -brass-type structure] [20].

For LiIn with NaTl-type structure, the lattice parameter  $a_{0K,0GPa}$  is calculated from the cubic root of  $8 \cdot V_o$  (Table 6). With  $V_o = 39.46 \text{ \AA}^3$ , a lattice parameter of  $a_{0K,0GPa} = 6.81 \text{ \AA}$  for LiIn is obtained. The tabulated lattice parameters [32, 33] for LiIn are  $a_{300K,1bar}$ : 6.792, 6.786, 6.7926, in  $\text{\AA}$ , with an average value of  $a_{300K,average} = 6.790 \text{ \AA}$ , leading to a unit-cell volume of  $V_{average300K} = 313.05 \text{ \AA}^3$  (with  $39.13 \text{ \AA}^3$ ,  $z = 1$ , 300 K). After correction for thermal expansion ( $38.52 \text{ \AA}^3$ , 10 K,  $z = 1$ , slightly tetragonal distorted NaTl-type structure for LiIn, Table 7) ( $38.52 - 39.13 = -0.61 \text{ \AA}^3$ ) with  $8 \cdot (-0.61) = -4.88 \text{ \AA}^3$  ( $313.05 - 4.88 = 308.17 \text{ \AA}^3$ ), a lattice parameter of  $a_{10K,1bar} = 6.75 \text{ \AA}$  is obtained for LiIn, in comparison with the WIEN2k value of  $a_{0K,0GPa} = 6.81 \text{ \AA}$ . Christensen had calculated a lattice parameter of  $a_{0K,0GPa} = 7.093 \text{ \AA}$  for LiIn [18]. The large deviation to the experimental

**Table 6** Calculated total energy  $E^0$  (Ryd), volume  $V_o(\text{\AA}^3)$  for one f.u., and bulk moduli  $B_o$  (GPa) of indides LiIn, NaIn, KIn, RbIn, and CsIn with the NaTl and the  $\beta$ -brass-type structure at zero pressure and temperature

	NaTl-type structure			$\beta$ -Brass-type structure		
	$E^0(\text{Ryd})$	$V_o(\text{\AA}^3)$	$B_o(\text{GPa})$	$E^0(\text{Ryd})$	$V_o(\text{\AA}^3)$	$B_o(\text{GPa})$
LiIn	-11,780.19109	39.46	36	-11,780.19223	37.69	35
NaIn	-12,089.71673	49.07	28	-12,089.69992	51.61	25
KIn	-12,968.81673	61.69	18	-12,968.78701	70.80	16
RbIn	-17,727.03623	68.20	16	-17,727.00640	79.47	14
CsIn	-27,344.10551	71.70	20	-27,344.07946	86.63	13

value ( $a_{\text{exp}} = 6.786 \text{ \AA}$ ) Christensen commented that he had “In treated as ‘frozen core’ states (causes overestimate of  $a_{\text{theor}}$ )” [18].

The tabulated lattice parameters [32, 33] for NaIn are  $a_{300\text{K},1\text{bar}}$ : 7.332 and 7.297, in  $\text{\AA}$ . The value of 7.297  $\text{\AA}$  has been determined by Zintl in 1933 [13], using a wavelength at that time of lower precision and may here be omitted. In the “Handbook for Intermetallic Phases,” first printing 1985 [32], there is a lattice parameter of NaIn (7.332  $\text{\AA}$ ) which is given twice from the measurements performed in 1970 and 1979 [32, 33]. With a value of  $a_{300\text{Kaverage}} = 7.332 \text{ \AA}$ , a unit-cell volume of  $V_{\text{average300K}} = 394.16 \text{ \AA}^3$  is obtained. After correction for thermal expansion, assuming proportionality between LiIn ( $-4.88 \text{ \AA}^3$  at  $313.05 \text{ \AA}^3$ , see above), a thermal correction of  $-\Delta V = -6.1 \text{ \AA}^3$  is calculated for NaIn with  $394.16 \text{ \AA}^3$  at 300 K. This leads to a corrected experimental lattice parameter at 10 K of NaIn of  $a_{10\text{K},1\text{bar}} = 7.29 \text{ \AA}$ . This value is in good agreement with the WIEN2k calculated value of  $a_{0\text{K},0\text{GPa}} = 7.30 \text{ \AA}$ . Christensen’s lattice parameter for NaIn of  $a_{0\text{K},0\text{GPa}} = 7.518 \text{ \AA}$  shows again a large deviation to his experimental value of 7.321  $\text{\AA}$  [18].

The differences in energy  $\Delta E^0$  and volume  $\Delta V_o$  between the phases with NaTl- and  $\beta$ -brass-type structure (Table 6) are strongly dependent on the size of the alkali metals, as also has been observed for the aluminides and gallides. Inspection of Table 6 and Fig. 10 shows that a structural change takes place for LiIn.

In Fig. 9, the total energies  $E^0$  are plotted as function of the volume. At 7.7 GPa, the NaTl phase has a volume of  $230 \text{ a.u.}^3 (=34.08 \text{ \AA}^3)$ , and the  $\beta$ -brass phase one of  $217 \text{ a.u.}^3 (=32.16 \text{ \AA}^3)$ . These values ( $34.08$  and  $32.16 \text{ \AA}^3$ ) can also be used to calculate the lattice parameters at 7.5 GPa and zero temperature. The cubic root of  $32.16 \text{ \AA}^3$  ( $z = 1$ ) is the lattice parameter  $a$  of the  $\beta$ -brass phase:  $a_{0\text{K}} = 3.18 \text{ \AA}$ . For the NaTl phase, one has to calculate the lattice parameter from  $8 \cdot 34.08 \text{ \AA}^3$  ( $z = 8$ ). The cubic root is  $a_{0\text{K}} = 6.48 \text{ \AA}$ . These values can be compared with the data of Schwarz et al. [20] who performed high pressure experiments (1998) on LiIn up to 18 GPa obtaining the  $\beta$ -brass phase from the NaTl phase. From their pressure–volume curve fitted to the experimental data, one can derive the volume, e.g., at 7.5 GPa. One obtains for the NaTl phase  $34.4 \text{ \AA}^3$  and for the  $\beta$ -brass phase  $33.3 \text{ \AA}^3$ . From these data, the lattice parameters at 7.5 GPa and 300 K  $a_{300\text{K}} = 3.22 \text{ \AA}$  for the  $\beta$ -brass phase and  $a_{300\text{K}} = 6.50 \text{ \AA}$  for the NaTl phase are derived. These data have to be corrected for thermal expansion with  $\Delta V = -0.73 \text{ \AA}^3$  for  $z = 1$  and

**Table 7** Space group, lattice parameter, volume for one f.u., and deviation from the ideal  $c/a$  ratio for LiIn obtained with Guinier diffractograms with  $CuK\alpha 1$  radiation in the temperature range between 300 and 10 K. The volume difference between 10 and 300 K is  $\Delta V = -0.73 \text{ \AA}^3$ 

T(K)	Space group	$a$ (Å)	$c$ (Å)	$c/(a\sqrt{2})$	$V$ (Å) <sup>3</sup>
10	I4 <sub>1</sub> /amd	4.7704(2)	6.7709(4)	1.0036	38.52(1)
30	I4 <sub>1</sub> /amd	4.7708(2)	6.7713(4)	1.0036	38.53(1)
50	I4 <sub>1</sub> /amd	4.7720(2)	6.7721(4)	1.0035	38.55(1)
100	I4 <sub>1</sub> /amd	4.7759(2)	6.7744(5)	1.0030	38.63(1)
200	Fd-3m	6.7809(3)			38.97(1)
300	Fd-3m	6.7970(3)			39.25(1)

a  $\Delta V = -0.73 \cdot 8 = -5.84 \text{ \AA}^3$  for  $z = 8$  (Table 7). The thermal corrected values of the lattice parameters of Schwarz et al. [20] are  $a_{10K,7.5GPa} = 3.19 \text{ \AA}$  and  $a_{10K,7.5GPa} = 6.46 \text{ \AA}$  which are in very good agreement with the values at 0 K  $a_{0K,7.5GPa} = 3.18 \text{ \AA}$  and  $a_{0K,7.5GPa} = 6.48 \text{ \AA}$ , calculated by WIEN2k.

However, for LiIn two other structures lie near to the energy minimum of –11,780.19223 Ryd (Table 6). These are the tetragonal distortions of the NaTl-type and of the  $\beta$ -brass-type structure. The tetragonal distortion the cubic NaTl-type structure was observed in 2002 by Ehrenberg et al. [19] as low temperature phase (see Sect. 4.3). The tetragonal distortion of the  $\beta$ -brass-type structure was obtained during our DAC experiments with LiTl (see Sect. 5.4). The transition temperature for cubic LiIn with the NaTl-type structure is 170(10) K [19]. In order to determine the thermal expansion, which is needed for comparison of the lattice parameters of  $A^I B^{III}$  phases at room temperature with those calculated by WIEN2k at zero temperature and pressure, cooling experiments down to 10 K have been performed on LiIn (Rotter, 2010, Department of Chemistry, LMU Munich, unpublished results) with X-ray Guinier diffractograms at 1 bar with  $CuK\alpha 1$  radiation. The results are summarized in Table 7. In agreement with the experiments of Ehrenberg et al. [19], the phase transition occurs between 200 and 100 K, and also the lattice parameter at 300 K  $a = 6.7970(3) \text{ \AA}$  (Table 7) by X-ray diffraction is in good agreement with those of Ehrenberg by neutron diffraction [6.7905(1) and 6.8014(3) Å, averaged to 6.7960 Å] [19]. At 10 K, the X-ray data are  $a = 4.7704(2)$ ,  $c = 6.7709(4) \text{ \AA}$  (Table 7) are also in good agreement with the averaged neutron data at 1.5 and 2 K ( $a = 4.7712$ ,  $c = 6.7835 \text{ \AA}$ ) [19], neglecting a temperature difference of approximately 8 K.

The deviation of the tetragonal lattice parameters of LiIn from the ideal ratio  $c/a = \sqrt{2}$  lies between 0.30% and 0.36% (Table 7). The splitting of the cubic 620 reflection (NaTl-type structure, high temperature phase) into the three tetragonal reflections 116, 332, and 420 (tetragonal distorted NaTl-type structure, low temperature phase) is shown in Fig. 11.

In Table 8 space group, calculated total energy  $E^o$ , volume  $V_o$  (Å<sup>3</sup>) for one f.u., and bulk modulus  $B_o$  (GPa) of LiIn, with the tetragonal distorted NaTl- and the tetragonal distorted  $\beta$ -brass-type structure (CuAu-type structure) at zero pressure and temperature, are summarized.

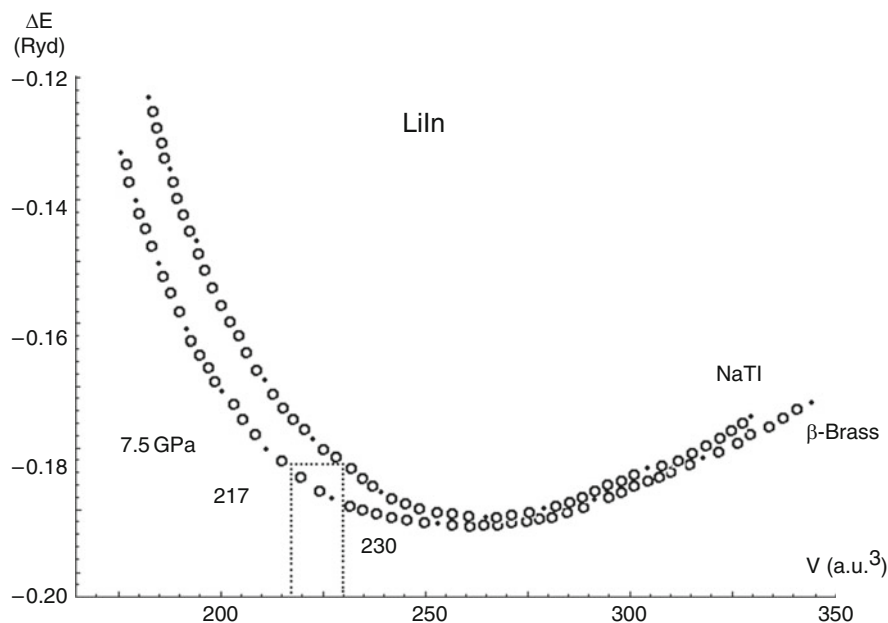


**Fig. 10** Total energy  $E^\circ$  (Ryd) curves for LiIn with the NaTl- and the  $\beta$ -brass-type as function of the unit-cell volume  $V$  (a.u.<sup>3</sup>). At 7.7 GPa, the NaTl-type structure of LiIn has a volume of 230 a.u.<sup>3</sup>, and the  $\beta$ -brass-type structure one of 217 a.u.<sup>3</sup>. From these data, the lattice parameters for both phases are derived (see text)

Comparison of Tables 6 and 8 shows that for LiIn the tetragonal distorted NaTl-type structure has  $0.07 \text{ \AA}^3$  lower calculated volume ( $= 0.2\%$ ) than the cubic phase. The total energy difference is zero, and the bulk moduli are practically equal (36, 37 GPa, respectively, Tables 6 and 8). The tetragonal distorted  $\beta$ -brass-type structure for LiIn has a  $0.18 \text{ \AA}^3$  lower volume ( $= 0.5\%$ ) than the cubic phase. The total energy difference for the two  $\beta$ -brass arrangements for LiIn is with 0.1 mRyd very low, and the bulk moduli are 35 GPa for the cubic phase and 39 GPa for the tetragonal distorted phase (Tables 6 and 8).

The energy differences between the NaTl- and the  $\beta$ -brass type for NaIn, KIn, RbIn, and CsIn are much higher than those for LiIn. They increase from  $-16.8$ ,  $-29.7$ ,  $-29.8$  and  $-26.0$  mRyd, respectively (Table 8), in comparison to  $+1.1$  mRyd for LiIn. Therefore, there it seems to be difficult to transform NaIn, KIn, RbIn, and CsIn with the NaTl-type structure into the  $\beta$ -brass-type structure in the pressure range up to 30 GPa.

The estimated energies of formation  $\Delta E_{f,AB}^\circ$  at zero temperature and pressure of NaTl-type phases for LiIn to CsIn and the estimated pressure (GPa) for stabilizing the NaTl-type structure in KIn to CsIn are summarized in Table 9.

For 1:1 alkali indides, LiIn and NaIn are the only stable phases with the NaTl-type structure at 1 bar. The estimated energies of formation (WIEN2k) at zero pressure and temperature  $\Delta E_{f,0K,0GPa}^\circ$  are  $-51$  and  $-18$  kJ/mole, respectively.

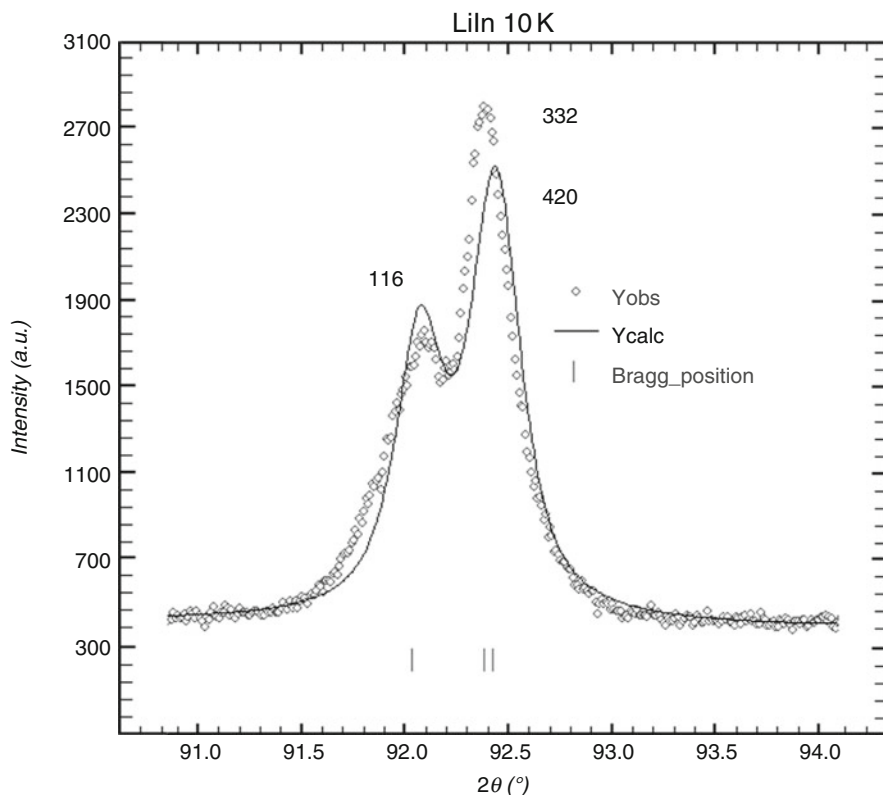


**Fig. 11** Section of the Guinier diffractogram ( $\text{CuK}\alpha 1$  radiation) at 10 K showing the splitting of the cubic 620 reflection into three tetragonal reflections 116, 332, and 420

With increasing metal radius from K to Cs, the estimated endergonic formation energies increase (+4, +21, +26 kJ/mole for KIn, RbIn, and CsIn, respectively; Table 8). There is good agreement found for the energy of formation  $\Delta E_{f,AB,0K,0G-Pa}^{\circ}$  (kJ/mole) for LiIn. By WIEN2k, a value of −51 kJ/mole was calculated. Predel's data are −49 kJ/mole (solution calorimetry) [29] and −46 kJ/mole (Miedema approach) [29, 30] (compare Sect. 2). The estimated stabilization pressure for the alkali indides KIn to CsIn with the NaTl-type structure lies in the range between 5 and 10 GPa (Table 9).

#### 5.4 *Thallides LiTl, NaTl, KTI, RbTl, and CsTl*

As in the cases of aluminides, gallides, and indides, in this chapter the total energy  $E^{\circ}$  calculations for thallides are presented, but in addition the results of high pressure in situ investigations in DAC on the thallides up to 30 GPa are given.

**Table 8** Space group, calculated total energy  $E^\circ$ (Ryd), volume  $V_o(\text{\AA}^3)$  for one f.u., and bulk modulus  $B_o$ (GPa) of LiIn, with the tetragonal distorted NaTl- and the tetragonal distorted  $\beta$ -brass-type structure (CuAu-type structure) at zero pressure and temperature

Tetragonal distorted NaTl-type structure			Tetragonal distorted $\beta$ -brass-type structure		
Space group I4 <sub>1</sub> /amd, LiIn			Space group P4/mmm, LiIn		
$E^\circ$ (Ryd)	$V_o(\text{\AA}^3)$	$B_o$ (GPa)	$E^\circ$ (Ryd)	$V_o(\text{\AA}^3)$	$B_o$ (GPa)
-11,780.19109	39.39	37	-11,780.19226	37.51	39

**Table 9** Estimated energy of formation  $\Delta E^\circ_{\text{AB},f,0\text{K},0\text{GPa}}$  (kJ/mole) for LiIn to CsIn and estimated pressure (GPa) for NaTl-type phases stabilized in KIn to CsIn

A <sup>I</sup> B <sup>III</sup> phase with NaTl-type structure	LiIn	NaIn	KIn	RbIn	CsIn
$\Delta E^\circ_{\text{AB},f,0\text{K},0\text{GPa}}$ (kJ/mole)	-51 <sup>a</sup>	-18	+4	+21	+26
Stabilization pressure (GPa)	0	0	5	10	5

<sup>a</sup> $\Delta H^\circ_{f,800\text{K}} = -49$  kJ/mole (solution calorimetry) [29],  $\Delta H^\circ_{f,300\text{K}} = -46$  kJ/mol (Miedema approach) [30]

The binary phase diagrams of the 1:1 alkali thallides show at 1 bar different types of phase diagrams [39]. As also observed for the compounds of lithium with aluminum, gallium, and indium, LiTl melts congruently at 520°C, also NaTl at 305°C. For KTl, a peritectical reaction at 268°C is found [39]. No compound RbTl is found in the Rb-Tl system, but for 50 Rb:50 Tl there is an eutecticum. Dong and Corbett prepared at ambient pressure KTl and CsTl, both phases with Tl<sub>6</sub>-octahedra [22, 25].

In Table 10, the calculated total energy  $E^\circ$ (Ryd), the volume  $V_o$  ( $\text{\AA}^3$ ), both for one f.u., and the bulk modulus  $B_o$  (GPa) for the thallides LiTl, NaTl, KTl, RbTl, and CsTl for the NaTl- and for the  $\beta$ -brass-type structure at zero pressure and temperature are summarized.

For the compounds LiTl and NaTl, both stable at ambient pressure, one calculates from the data of Table 10 the lattice parameters  $a_{0\text{K},0\text{GPa}} = 3.43$   $\text{\AA}$  for LiTl with the  $\beta$ -brass-type structure and  $a_{0\text{K},0\text{GPa}} = 7.50$   $\text{\AA}$  for NaTl with the NaTl-type structure. The tabulated lattice parameter [32, 33] for LiTl is  $a_{300\text{K},1\text{bar}} = 3.431$   $\text{\AA}$  and for NaTl it is  $a_{300\text{K},1\text{bar}} = 7.469$  [32], 7.462, 7.488, 7.448 [33]  $\text{\AA}$ , with an average value of 7.467  $\text{\AA}$  leading to unit-cells with a volume of 40.39 and 416.3  $\text{\AA}^3$ , respectively. After correction for thermal expansion,  $a_{10\text{K},1\text{bar}} = 3.41$   $\text{\AA}$  (LiTl) and  $a_{10\text{K},1\text{bar}} = 7.42$   $\text{\AA}$  (NaTl) are obtained. The calculated lattice parameters of Schmidt are  $a_{0\text{K},0\text{GPa}} = 3.425$   $\text{\AA}$  (LiTl) and  $a_{0\text{K},0\text{GPa}} = 7.488$   $\text{\AA}$  (NaTl) [9]. From Christensen [18], only the lattice parameter of NaTl ( $a_{0\text{K},0\text{GPa}} = 7.439$   $\text{\AA}$ ) can be compared here, because for LiTl an erroneous value of  $a_{0\text{K},0\text{GPa}} = 6.883$   $\text{\AA}$  is listed in Table 3. This value must belong to a not stable NaTl-type structure for LiTl.

As it has been also observed for aluminides, gallides, and indides, the differences in energy  $\Delta E^\circ$  and volume  $\Delta V_o$  between the phases with NaTl- and  $\beta$ -brass-type structure (Table 10) are strongly size dependent, having in mind that LiTl with  $\beta$ -brass-type structure is -10.6 mRyd more stable than NaTl-type phase.



**Table 10** Calculated total energy  $E^o$ (Ryd), volume  $V_o(\text{\AA}^3)$ , and bulk moduli  $B_o$  (GPa) for one f.u. of thallides LiTl, NaTl, KTl, RbTl, and CsTl with the NaTl- and the  $\beta$ -brass-type structure at zero pressure and temperature

	NaTl-type structure			$\beta$ -Brass-type structure		
	$E^o$ (Ryd)	$V_o(\text{\AA}^3)$	$B_o$ (GPa)	$E^o$ (Ryd)	$V_o(\text{\AA}^3)$	$B_o$ (GPa)
LiTl	-40,590.24904	43.24	31	-40,590.25935	40.20	32
NaTl	-40,899.78644	52.67	24	-40,899.78043	53.79	22
KTl	-41,778.89178	65.25	15	-41,778.87256	72.57	13
RbTl	-46,537.11216	71.23	14	-46,537.09218	80.02	13
CsTl	-56,154.18300	74.35	19	-56,154.15965	83.59	14

Christensen calculated this energy difference to  $-8.6$  mRyd [18], and Schmidt with the scalar relativistic augmented-plane-wave method (SRAPW) to  $-11.0$  mRyd [9]. From NaTl to CsTl, the differences in energy and volume increase (Table 10). For NaTl, the energy difference is  $\Delta E^o = -6.0$  mRyd and the difference in volume  $\Delta V_o = -1.12 \text{ \AA}^3$ ; for CsTl these values are  $-23.3$  mRyd and  $-9.24 \text{ \AA}^3$ , respectively. For NaTl, this energy difference was calculated by Christensen to  $-8.8$  mRyd [18] and by Schmidt to  $-0.4$  mRyd [9].

Inspection of Table 10 shows also that LiTl with the NaTl-type and the  $\beta$ -brass-type structure has the highest bulk moduli  $B_o$  (31, 32 GPa, respectively) of the thallides series. Christensen calculated the bulk modulus  $B_o$  of LiTl with the  $\beta$ -brass-type structure to 35.7 GPa [18] and for NaTl with the NaTl-type structure to 29.9 GPa. The LiTl phases are therefore the hardest materials for the alkali thallides. Interestingly, LiTl is the only exception for the  $A^I B^{III}$  phases, calculated here with WIEN2k, where the  $\beta$ -brass-type phase has a higher bulk modulus  $B_o$  (32 GPa) than the NaTl-type phase (31 GPa, Table 10). Again the bulk modulus of CsTl (NaTl-type structure) is higher than for RbTl as it is also observed for CsIn (NaTl-type structure) in comparison to RbIn (Table 6).

In Table 11, the estimated energies of formation  $\Delta E_{AB,f,0K,0GPa}^o$  (kJ/mole) at zero temperature and pressure and the estimated stabilization pressure to obtain the NaTl-type structure are summarized. For 1:1 alkali thallides, there are only two stable phases, 1 bar: LiTl with the  $\beta$ -brass- and NaTl with NaTl-type structure. The estimated energies of formation (WIEN2k) at zero pressure and temperature  $\Delta E_{f,0K,0GPa}^o$  are  $-42$  and  $-10$  kJ/mole, respectively (Table 11). There is good agreement for the energy of formation  $\Delta E_{f,AB,0K,0GPa}^o$  (kJ/mole) for LiTl. By WIEN2k, a value of  $-42$  kJ/mole was obtained, Predel's data are  $-40$  kJ/mole (solution calorimetry) [29] and  $-55$  kJ/mole (Miedema approach) [29, 30]. With increasing metal radius from K to Cs, the endergonic formation energies increase ( $+4$ ,  $+19$ ,  $+23$  kJ/mole for KTl, RbTl, and CsTl with the NaTl-type structure, respectively). The estimated stabilization pressure for these NaTl-type phases is about 5 GPa (Table 11). This is in good agreement with the facts that in the DAC experiments these phases can be obtained with the NaTl-type structure at "low" high pressures.

**Table 11** Estimated energy of formation  $\Delta E^\circ_{f,AB,0K,0GPa}$  (kJ/mole) for LiTl with the  $\beta$ -brass-, for NaTl, KTl, RbTl, and CsTl with the NaTl-type structure and estimated pressure (GPa) for NaTl-type phases stabilized in KTl to CsTl

A <sup>I</sup> B <sup>III</sup> phase with NaTl-type structure	LiTl <sup>a</sup>	NaTl	KTl	RbTl	CsTl
$\Delta E^\circ_{f,AB,0K,0GPa}$ (kJ/mole)	-42 <sup>b</sup>	-10	+4	+19	+23
Stabilization pressure (GPa)	0	0	5	5	5

<sup>a</sup>LiTl with  $\beta$ -brass-type structure

<sup>b</sup> $\Delta H^\circ_{f,800K} = -40$  kJ/mole (solution calorimetry) [29],  $\Delta H^\circ_{f,300K} = -55$  kJ/mol (Miedema approach) [30]

Figure 12 shows that the  $\beta$ -brass-type phase for LiTl is lower in energy and volume. Therefore, at high pressure the  $\beta$ -brass type cannot be transformed in the investigated high pressure range up to 40 GPa into the NaTl-type structure.

The investigations in the DAC showed that the cubic  $\beta$ -brass-type structure of LiTl can be transformed into the tetragonal AuCu-type structure. The WIEN2k calculations showed that the equilibrium volume  $V_o$  for the AuCu phase ( $40.29 \text{ \AA}^3$ ) is  $0.09 \text{ \AA}^3$  slightly higher than that of the cubic  $\beta$ -brass-type phase of LiTl ( $V_o = 40.20 \text{ \AA}^3$ ). The difference in total energies is with  $0.1 \text{ mRyd}$  also very small. The  $\beta$ -brass-type phase is  $-0.6 \text{ mRyd}$  more stable than the AuCu phase, having in mind that the NaTl-type phase of LiTl is with  $+10.3 \text{ mRyd}$  less stable than the cubic  $\beta$ -brass-type phase (Table 10). The differences in energy and volume between the cubic  $\beta$ -brass-type structure and its tetragonal distortion are too small to be displayed with the scale of Fig. 12.

The DAC experiments on LiTl showed that at pressures up to 31.0(10) GPa both, the  $\beta$ -brass-type structure and the AuCu-type structure, are obtained. Figure 13 shows the Rietveld plot obtained at 21.0(8) GPa, analyzed with FullProf [28]. The lattice parameter for LiTl with the cubic  $\beta$ -brass- and the tetragonal AuCu-type structure up to 31.0(10) GPa is summarized in Table 12. Inspection of this table shows that the tetragonal phase has a slightly smaller unit-cell volume than the cubic one, e.g.,  $26.3(5)$  and  $27.8(3) \text{ \AA}^3$ , respectively, at 31.0(10) GPa (Table 12). The averaged axial ratio  $a/c$  is 1.48. Calculation of the axial ratio at constant volume with WIEN2k resulted in a ratio  $a/c$  of 1.46.

The Rietveld analysis of the AuCu-type structure of LiTl at high pressure showed that 30% of the Tl atoms are distributed on Li positions. A lot of compression and decompression cycles of the LiTl sample in the DAC did not improve the ordering of the Li and the Tl atoms in the CuAu-type structure phase.

Interestingly, at ambient pressure Zintl, Brauer, and Dullenkopf determined a tetragonal distorted CsCl structure ( $\beta$ -brass-type structure) for the A<sup>I</sup>B<sup>V</sup> compounds LiBi ( $a_{CsCl} = 3.361$ ,  $c = 4.247 \text{ \AA}$ ) [37] and for NaBi ( $a_{CsCl} = 3.46$ ,  $c = 4.80 \text{ \AA}$ ) [38] with one f.u./cell ( $z = 1$ ). These lattice parameters can be transformed into that of the AuCu-type structure with  $z = 2$ . This results into the lattice parameters for LiBi with  $a = 4.753$ ,  $c = 4.247 \text{ \AA}$  ( $a/c = 1.12$ ) and for NaBi with  $a = 4.89$ ,  $c = 4.80 \text{ \AA}$  ( $a/c = 1.02$ ) (Table 13). These lattice parameters for LiBi and NaBi can now be compared with the calculated lattice parameters for the AuCu-type structures in A<sup>I</sup>B<sup>III</sup> compounds LiTl and NaTl.

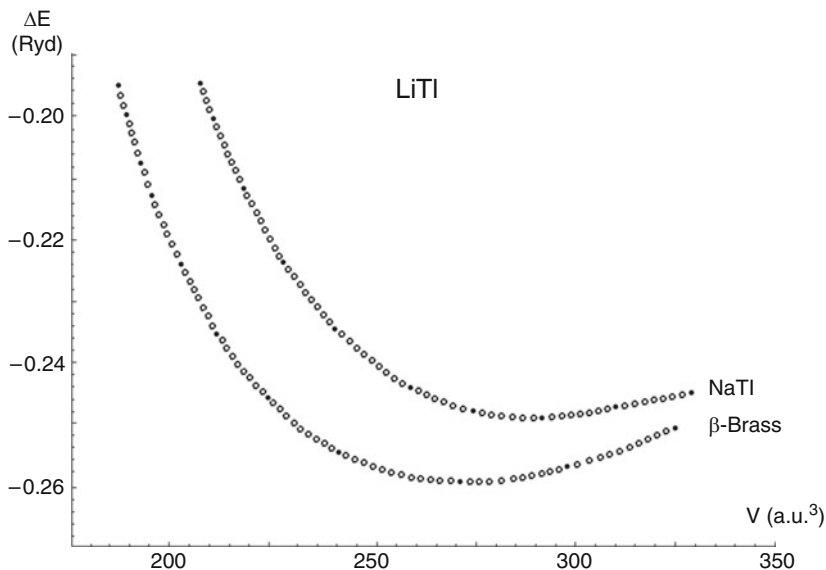


**Fig. 12** Total energy  $E^\circ$  (Ryd) curves for LiTl with the  $\beta$ -brass- and the NaTl-type as function of the unit-cell volume  $V$  (a.u.<sup>3</sup>). The  $\beta$ -brass type is lower in energy and in volume and cannot be transformed into the NaTl-type structure

The  $a/c$  ratio for LiTl and NaTl is with 1.46 remarkably larger than that for LiBi and NaBi with 1.12 and 1.02, respectively (Table 13). The lattice parameters for axis  $a$  (Å) have comparable size (4.753–5.38), but the lattice parameters for axis  $c$  the thallides are approximately 1 Å smaller than the bismuthides. The smaller  $c$ -axis in LiTl and NaTl leads to eight smaller A-B contacts in the thallides (2.97, 3.26 Å) and then in the bismuthides (3.19, 3.43 Å).

It is useful to compare now the A-B distances in the two phases of LiTl, one with the AuCu- and the other with the  $\beta$ -brass-type structure at 31.0(10) GPa. For the AuCu-type structure, an ordered distribution of Li and Tl atoms is assumed. With the lattice parameter 3.03(1) Å for the  $\beta$ -brass-type phase (Table 12), eight LiTl distances of 2.62(1) Å could be achieved. For the AuCu-type structure with the lattice parameters of 4.28(2) and 2.87(2) Å, eight LiTl distances of 2.58(1) Å could be realized under ideal conditions of ordered distribution of atoms. At 31.0(10) GPa, the LiTl distance in the AuCu-type structure, the eight LiTl distances are with 0.04 Å slightly smaller than in the  $\beta$ -brass-type structure. Therefore, this structure could be the end member obtained by very high pressure treatment of  $A^I B^{III}$  compounds with small radius ratio  $r_A/r_B$ , e.g., for lithium and the sodium compounds of this series. For larger  $A^I$  metals like potassium, rubidium, and cesium, the NaTl-type structure is favored as the DAC investigations for NaTl, KTI, and RbTI show in the following.

The difference between the NaTl-type and  $\beta$ -brass structure in NaTl is only –6.0 mRyd with the first also lower in volume (Table 10). With increasing pressure the

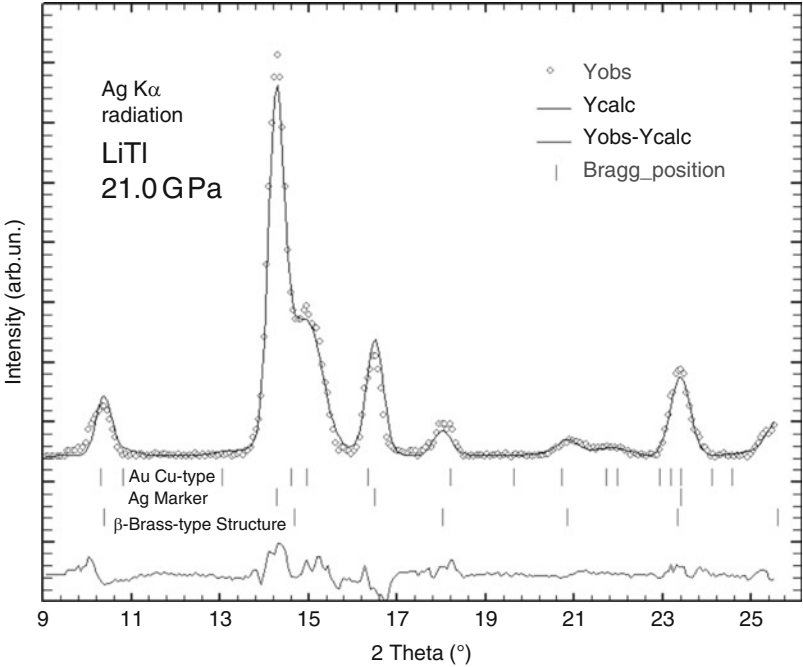


**Fig. 13** Rietveld plot with FullProf [28] for LiTi with the  $\beta$ -brass- and the AuCu-type structure at 21.0 GPa (DAC diffractometer, Ag K $\alpha$  radiation with 0.5609 Å). The measured data are shown as circles, the calculated diffractogram is shown as dark, the difference as gray line. The calculated 2-theta values are shown as vertical bars. Silver was used as internal pressure marker. The lattice parameter of silver at ambient pressure is  $a = 4.0853$  Å, at the applied pressure in the DAC it is  $a = 3.905$  Å. With  $d/d^0 = 3.905/4.0853 = 0.9559$ , the applied pressure is 21.0(8) GPa [27]

**Table 12** Lattice parameters of LiTi with the  $\beta$ -brass- and the AuCu-type structure to 31.0 GPa

$p$ (GPa)	$\beta$ -Brass-type structure		AuCu-type structure			
	$a$ (Å)	$V$ (Å <sup>3</sup> )	$a$ (Å)	$c$ (Å)	$a/c$	$V$ (Å <sup>3</sup> )
LiTi						
0.0001	3.4332(5) <sup>a</sup>	40.47(1)				
5.2(3)	3.26(1)	34.6(3)				
11.0(5)	3.20(1)	32.8(3)	4.54(2)	3.07(2)	1.48	31.6(5)
12.8(5)	3.17(1)	31.9(3)	4.53(2)	3.05(2)	1.49	31.3(5)
14.0(6)	3.16(1)	31.6(3)	4.49(2)	3.03(2)	1.48	30.5(5)
21.0(8)	3.10(1)	29.8(3)	4.40(2)	2.98(2)	1.48	28.8(5)
24.5(8)	3.07(1)	28.9(3)	4.36(2)	2.94(2)	1.48	27.9(5)
31.0(10)	3.03(1)	27.8(3)	4.28(2)	2.87(2)	1.49	26.3(5)

<sup>a</sup>1 bar, Guinier diffractogram

difference in energy and volume decrease, as it is shown in Fig. 14. Here the total energy  $E^0$  is plotted as function of the volume. At about 210 a.u.<sup>3</sup> ( $= 31.12$  Å<sup>3</sup>), the energy curves touch each other at about 40 GPa. At this volume both phases should be in equilibrium.

**Table 13** Tetragonal lattice parameters  $a$  and  $c$ , axial ratio  $a/c$ , and volume  $V$  ( $z = 1$ ) for four phases with the AuCu-type structure: LiBi and NaBi at ambient conditions [37, 38], LiTl and NaTl calculated with WIEN2k at zero pressure and temperature

	LiTl	LiBi	NaTl	NaBi
$a(\text{\AA})$	4.90	4.753	5.38	4.89
$c(\text{\AA})$	3.35	4.247	3.68	4.80
$a/c$	1.46	1.12	1.46	1.02
$V(\text{\AA}^3)$	40.29	47.97	53.25	57.39
8 A-B ( $\text{\AA}$ )	2.97	3.19	3.26	3.43

In Fig. 15, the Rietveld plot for NaTl with the NaTl- and the  $\beta$ -brass-type structure at 25.5 GPa is shown.

In Table 14, the lattice parameters of NaTl with the NaTl- and with the  $\beta$ -brass-type structure up to 32.5 GPa are summarized.

Inspection of Table 14 shows the lattice parameters of NaTl with the NaTl- and with the  $\beta$ -brass-type structure up to 32.5 GPa. The novel  $\beta$ -brass-type phase for NaTl created at high pressure has a statistical distribution of Na and Tl atoms. Annealing did not improve the ordering. NaTl, although not ordered, is after LiTl and LiIn the third  $A^I B^{III}$  phase with  $\beta$ -brass-type structure.

In Fig. 16, the total energy  $E^0$  curves for KTl with the orthorhombic ambient pressure phase with isolated  $\text{Ti}_6$ -octahedra [22], the NaTl- and the  $\beta$ -brass-type structure are shown.

In the earlier HP investigation on KTl in our group [21], a Rietveld plot obtained at 4.5 GPa had been published. In this investigation, the pressure has been largely increased. In Fig. 17, the Rietveld plot for the diffractogram of KTl obtained in the DAC diffractometer at 24.5 GPa is displayed, and in Table 15 the lattice parameter and volume ( $\text{\AA}^3$ ) for  $z = 1$  are summarized. No  $\beta$ -brass-type phase could be obtained for KTl up to 30 GPa since here the differences in energy between both structures  $\Delta E^0 = -19.2$  mRyd (Table 10) are too large. The NaTl-type structure of KTl could be stored at ambient pressure after total pressure release. Diffractograms at 1 bar indicated a mixture of the cubic and the orthorhombic phase. The cubic phase remained for few days, and after this time only the orthorhombic phase was observed.

For KTl with the NaTl-type structure and also with the  $\beta$ -brass-type structure, electron density maps have been calculated with WIEN2k, both at 0 and 30 GPa. The contour line shows the calculated electron densities with increasing electron density from 0.05 to 0.95 in  $\text{e}/\text{\AA}^3$  (Figs. 18 and 19).

In Fig. 18, views are displayed on the (110) plane of KTl with the NaTl-type structure with zigzag chains of four Tl atoms with four adjacent K atoms. At 0 GPa (Fig. 18a), a contour line of  $0.1 \text{ e}/\text{\AA}^3$  surrounds the four Tl atoms indicating covalent bonding between them. The Tl–Tl bond distance in KTl at 0 GPa is  $3.47 \text{ \AA}$ , and the unit-cell volume  $514 \text{ \AA}^3$ . Between the Tl and the K atoms, there are kidney-shaped areas with a contour line of  $0.05 \text{ e}/\text{\AA}^3$  probably resulting from polarizing effects of the K ions on the valence electrons of the Tl polyanion [20].

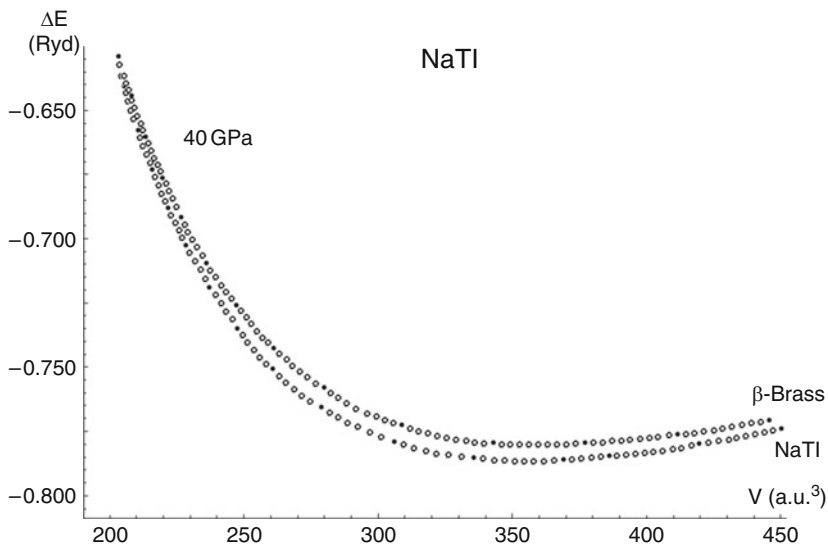


**Fig. 14** Total energy  $E^0$  (Ryd) curves for NaTl with the NaTl- and the  $\beta$ -brass as function of the unit-cell volume  $V$  (a.u.<sup>3</sup>). At approximately 210 a.u.<sup>3</sup>, the NaTl- and the  $\beta$ -brass-type structure should be in equilibrium

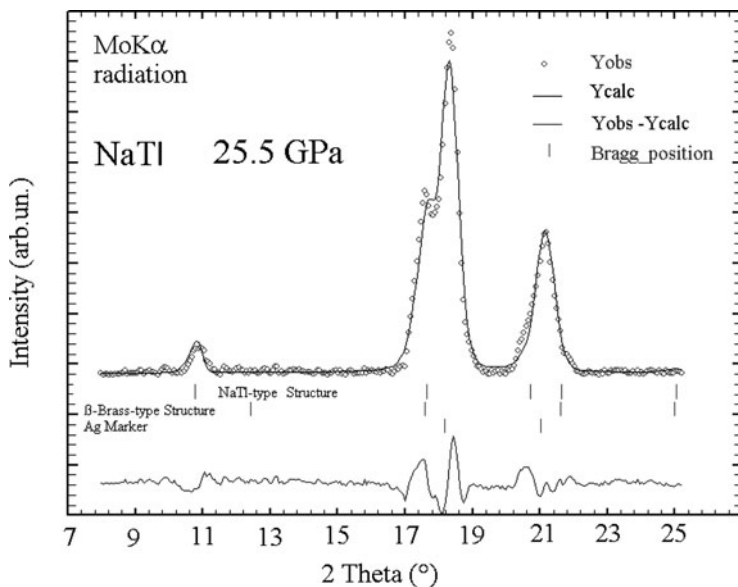


**Fig. 15** Rietveld plot with FullProf [28] for NaTl with the NaTl- and the  $\beta$ -brass-type structure at 25.5 GPa (DAC diffractometer, MoK $\alpha$  radiation with 0.7107 Å). The measured data are shown as circles, the calculated diffractogram is shown as dark, and the difference as gray line. The calculated 2-theta values are shown as vertical bars. Silver was used as internal pressure marker

**Table 14** Lattice parameter of NaTl with the NaTl- and the  $\beta$ -brass-type structure up to 32.5 GPa, obtained by Rietveld analysis of the DAC diffractograms

$p$ (GPa)	NaTl-type structure		$\beta$ -Brass-type structure	
	$a(\text{\AA})$	$V(\text{\AA}^3)$	$a(\text{\AA})$	$V(\text{\AA}^3)$
0.001	7.482(2) <sup>a</sup>	52.36(4)		
0.5(2)	7.47(2)	51.1(3)		
3.2(3)	7.20(2)	46.7(3)	3.64(1)	48.2(1)
6.5(3)	7.06(2)	44.0(3)	3.52(1)	43.6(1)
16.0(6)	6.68(2)	37.3(3)	3.35(1)	37.6(1)
18.0(6)	6.66(2)	36.9(3)	3.32(1)	36.6(1)
22.0(8)	6.59(2)	35.8 (3)	3.29(1)	35.6(1)
25.5(8)	6.56(2)	35.3(3)	3.28(1)	35.3(1)
32.5(10)	6.43(2)	33.2(3)	3.20(1)	32.8(1)

<sup>a</sup>1 bar, Guinier diffractogram

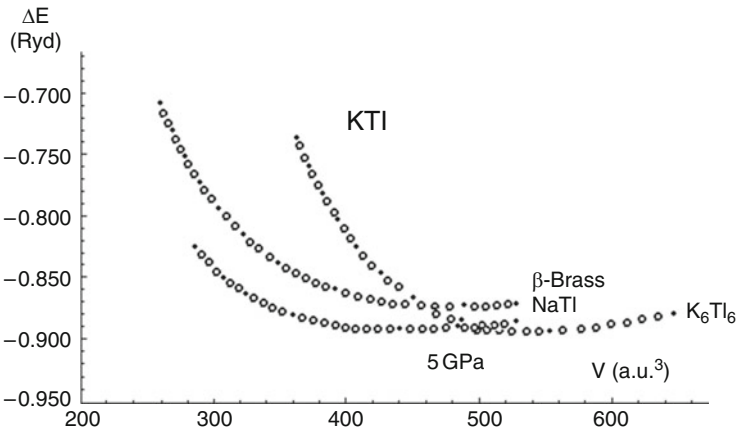


**Fig. 16** Total energy  $E^0$  (Ryd) curves for KTI with the NaTl-, the  $\beta$ -brass- and the orthorhombic normal pressure phase, which contains isolated  $Tl_6$ -octahedra [22], are shown as function of the volume  $V$  (a.u.<sup>3</sup>). At 480 a.u.<sup>3</sup> ( $= 71.12 \text{\AA}^3$ ), the curve of the orthorhombic phase intersects the curve for NaTl-type phase. The NaTl-type structure for KTI is then lower in energy and volume. From the Murnaghan fit [34] for the orthorhombic phase, a pressure of 5 GPa is derived

At 30 GPa (Fig. 18b), KTI with the NaTl-type structure is compressed (−40%) to a unit-cell volume of only  $306 \text{\AA}^3$  with a Tl–Tl bond distance of  $2.92 \text{\AA}$ . The 32 valence electrons in the unit-cell are now distributed into a smaller unit-cell. Now three contour lines of 0.1, 0.25, and  $0.30 \text{ e/\AA}^3$  surround the zigzag chain of four Tl atoms, indicating that even at 30 GPa KTI is even a Zintl compound  $K^+Tl^-$  with four covalent Tl–Tl bonds. In comparison to Fig. 18a, the kidney-shaped areas between the Tl and the K atoms are now increased in Fig. 18b and show a contour line of  $0.15 \text{ e/\AA}^3$ , indicating an increased polarizing effect of the K ions.

In Fig. 19, views are displayed on the (110) plane of KTI with the  $\beta$ -brass-type structure. KTI with this structure is endergonic up to 30 GPa and could therefore not

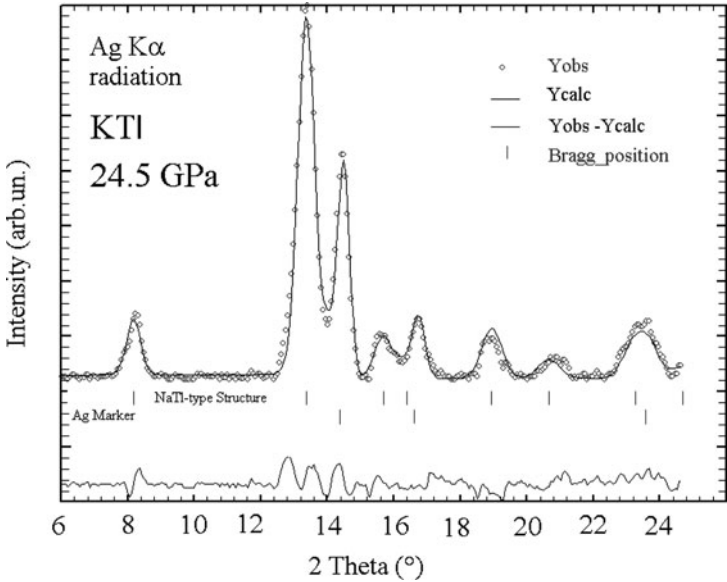


**Fig. 17** Rietveld plot with [28] for KTI with the NaTi-type structure at 24.5 GPa (DAC diffractometer, Ag K $\alpha$  radiation with 0.5609 Å). The measured data are shown as *circles*, the calculated diffractogram is shown as *dark*, the difference as *gray line*. The calculated 2-theta values are shown as *vertical bars*. Silver was used as internal pressure marker

**Table 15** Lattice parameter of KTI with the NaTi-type structure up to 24.5 GPa, obtained by Rietveld analysis of the DAC diffractograms. The lattice parameter at 1 bar (0.0001 GPa) was obtained from a mixture with the orthorhombic phase [22] when the pressure was completely released

<i>p</i> (GPa)	NaTi-type structure	
KTI	<i>a</i> (Å)	<i>V</i> (Å <sup>3</sup> )
0.0001	8.01(2)	64.2(5)
2.4(3)	7.81(2)	59.5(5)
3.0(3)	7.69(2)	56.8(5)
3.7(3)	7.63(2)	55.5(5)
7.2(4)	7.43(2)	51.3(5)
8.0(4)	7.40(2)	50.7(5)
14.6(6)	7.08(2)	44.4(5)
24.5(8)	6.82(2)	39.7(5)

be prepared in a DAC at this pressure. At 0 GPa (Fig. 19a), the Tl and the K atoms show a nearly spherical charge distribution with contour lines increasing from 0.1, 0.15, and 0.2 e/Å<sup>3</sup> to much higher values. Between the Tl and the K atoms, there are areas found with a contour line of 0.1 e/Å<sup>3</sup>. These areas do not touch neither the Tl nor the K atoms. The unit-cell volume is 70.8 Å<sup>3</sup>. At 30 GPa (Fig. 19b), the unit-cell volume of KTI with the  $\beta$ -brass type is compressed (−40%) to 41.4 Å<sup>3</sup>. The Tl and the K atoms show also a nearly spherical charge distribution, but now with contour lines increasing from 0.2, 0.25, and 0.3 e/Å<sup>3</sup> to much higher values. Between the



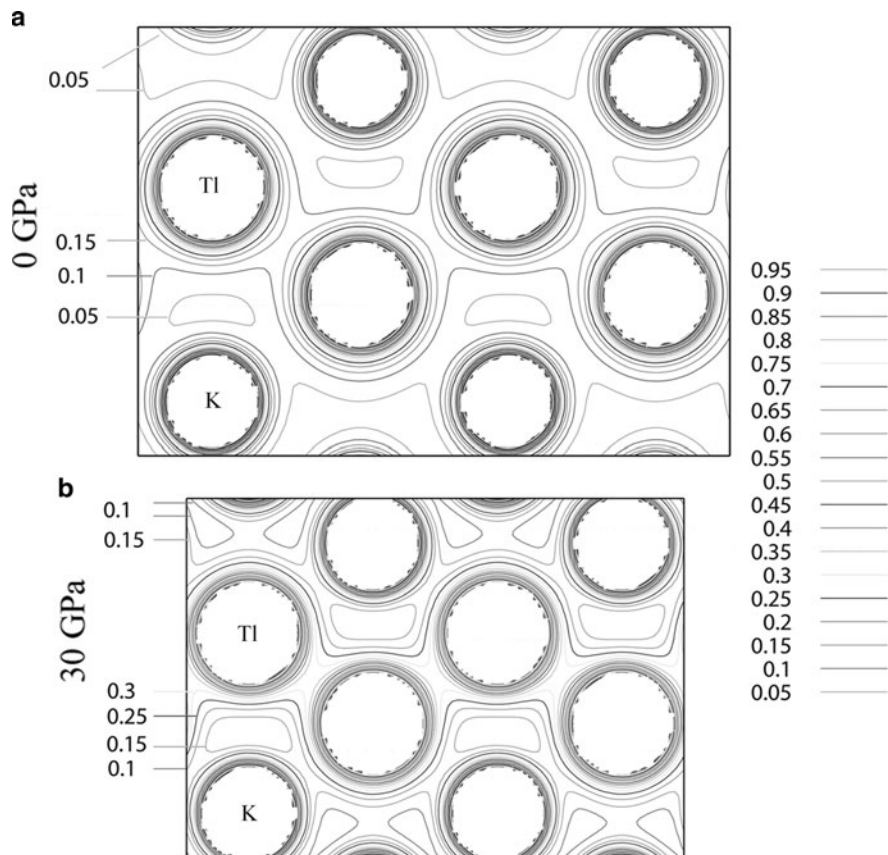


**Fig. 18** Electron density maps for KTI with the NaTI-type structure [23] shown for the (110) plane with a zigzag chain of four Tl atoms and four adjacent K atoms. Isolines are in equal steps of  $\approx 0.05 \text{ e}/\text{\AA}^{-3}$  increasing from 0.05 to 0.95 in  $\text{e}/\text{\AA}^3$  (a) at 0 GPa and (b) at 30 GPa

Tl and the K atoms, there are areas with contour lines of  $0.1 \text{ e}/\text{\AA}^3$ . Interestingly, a second contour line of  $0.15 \text{ e}/\text{\AA}^3$ , lying between these atoms, occurs now. These lines surround now the Tl and also the four K atoms, probably indicating weak metallic bonding between them.

In Table 16, for RbTI with NaTI-type structure, the lattice parameters  $a(\text{\AA})$  and the volume  $V(\text{\AA}^3)$  for one formula up to 16.8(6) GPa are summarized. Fitting of the four experimental pressure–volume data of Table 16 with the Murnaghan equation [34] leads to a lattice parameter of  $a = 8.37(4) \text{ \AA}$  at 1 bar and 300 K. By correction of this value by thermal expansion (derived from the thermal expansion of LiIn), a value of  $a_{10\text{K}, 1\text{bar}} = 8.32 \text{ \AA}$  is derived. By calculation with WIEN2k (Table 10),  $a_{0\text{K}, = \text{GPa}} = 8.29 \text{ \AA}$  is obtained.

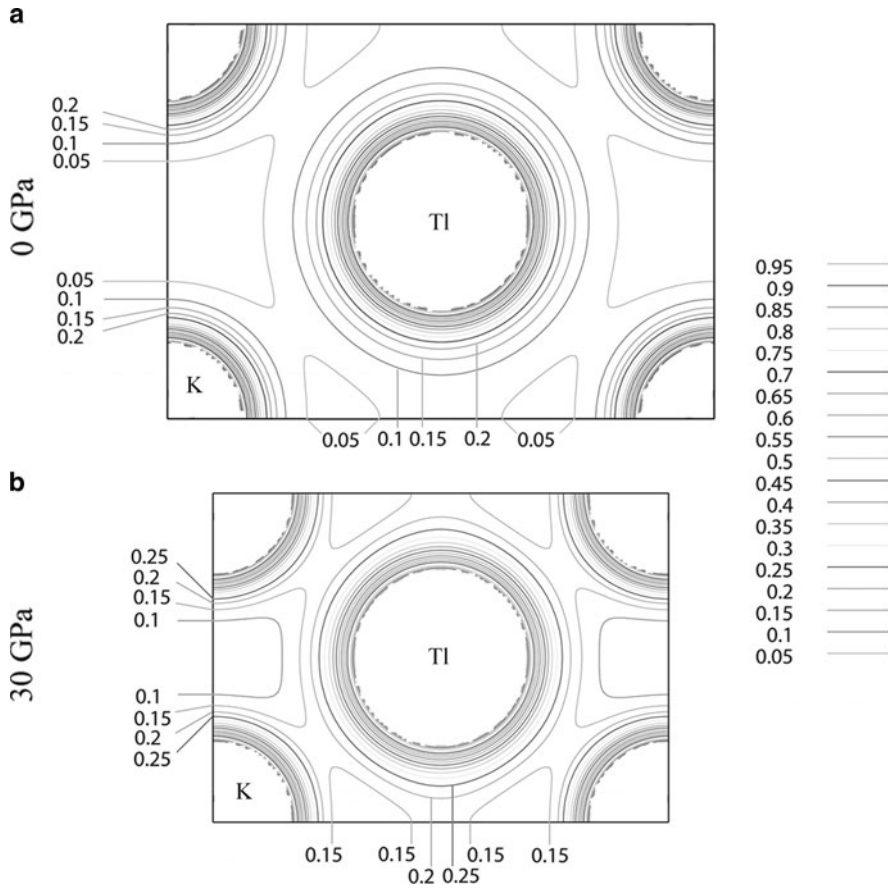


**Fig. 19** Electron density maps for KTi with the  $\beta$ -brass-type structure [23] shown for the (110) plane. Isolines are in equal steps of  $\approx 0.05 \text{ e}/\text{\AA}^3$  increasing from 0.05 to 0.95 in  $\text{e}/\text{\AA}^3$  (a) at 0 GPa and (b) at 30 GPa

By the DAC experiments for CsTi, only diffractograms of low quality, showing strong texture, were obtained. Annealing at about  $100^\circ\text{C}$  did not improve their quality. Lattice parameters for CsTi with the NaTi-type structure could be derived indexing the strong reflection as 220. At 21 GPa, a lattice parameter of  $7.23(8) \text{ \AA}$  and at 4 GPa one of  $8.07(8) \text{ \AA}$ . From  $V_o = 74.35 \text{ \AA}^3$  obtained with WIEN2k for CsTi (Table 10), a lattice parameter of  $a_{0\text{K},0\text{GPa}} = 8.41 \text{ \AA}$  is derived. Correction for thermal expansion leads to  $a_{300\text{K},1\text{bar}} = 8.37 \text{ \AA}$  for CsTi with the NaTi-type structure.

The estimations of the energy of formation for the  $\text{A}^{\text{I}}\text{B}^{\text{III}}$  compound with WIEN2k have been internally standardized against the heats of formation obtained by solution calorimetry and its estimation by the Miedema approach of LiIn and LiTi, both from Predel's group. Six  $\text{A}^{\text{I}}\text{B}^{\text{III}}$  of total 20 compounds are stable at 0 K,

**Table 16** Lattice parameter of RbTl with the NaTl-type structure up to 16.8 GPa, obtained by Rietveld analysis of the DAC diffractograms. The parameter at 1 bar (0.0001 GPa) was calculated with WIEN2k and then corrected for thermal expansion with the data of LiIn

$p$ (GPa)	NaTl-type structure	
RbTl	$a(\text{\AA})$	$V(\text{\AA}^3)$
0.0001	8.37(4) <sup>a</sup>	73.3(10)
0.6(2)	8.01(2)	64.2(5)
7.6(3)	7.66(2)	56.2(5)
14.5(6)	7.48(2)	52.3(5)
16.8(6)	7.32(2)	49.0(5)

<sup>a</sup>8.32 Å calculated for 10 K, 0 bar, corrected for thermal expansion +10.38 Å<sup>3</sup> from LiIn-data +5.84 Å<sup>3</sup>

0 GPa (LiAl, LiGa, LiIn, LiTl and NaIn, NaTl) in agreement with Zintl's classical investigations. The remaining 14  $A^I B^{III}$  compounds are endergonic at zero pressure and temperature. The estimations show that in the pressure range up to 30 GPa, the NaTl-type structure could be stabilized. The lowest pressure (5 GPa) for stabilizing the NaTl-type structure is estimated for NaGa, KTI, RbTl, CsIn, and CsTl, and the highest pressure (30 GPa) for KAl, RbAl, and CsAl (Tables 3, 5, 9, and 11).

The lattice parameters calculated with WIEN2k (0 K, 0 GPa) deviate for LiAl, LiGa, LiIn, LiTl, NaIn, and NaTl from the experimental values (300 K 0.0001 GPa) after correction for thermal expansion only few on the second digit. For LiAl, the calculated lattice parameter with WIEN2k (0 K, 0 GPa) is 6.33 Å, and the experimental lattice parameter (10 K, 0.0001 GPa) is also 6.33 Å. For LiGa, LiIn, LiTl, NaIn, and NaTl, the analogous data in Å are 6.18/6.15, 6.81/6.75, 3.43/3.41, 7.30/7.29, and 7.50/7.42. Also the calculated lattice parameters of LiIn at 7.5 GPa, both for the NaTl- and the  $\beta$ -brass-type structure, are in very good agreement with the DAC experiments [20]. Therefore, there are now lattice parameters at 0 GPa available for 19  $A^I B^{III}$  compounds with the NaTl-type structure with sufficient precision. LiTl with  $\beta$ -brass-type structure is more stable than that with the NaTl-type structure and is not considered here.

These data can be used to construct the near-neighbor diagram for the NaTl-type structure. Pearson had introduced such diagrams to get information which factors control intermetallic compounds with specific structures, e.g., a geometrical or a chemical bond factor [40–43]. Beside several intermetallic structures, e.g., the Laves phases, the  $\sigma$ -phases, and the CrB-phases, Pearson investigated also the NaTl-type structure for  $A^I B^{III}$  compounds and, in addition, for LiZn and LiCd. For the  $A^I B^{III}$  compounds, he corrected the radii for  $r_{AI}$  and  $r_{BIII}$  given by Teatum and Gschneidner [43–45] to coordination number eight and calculated with the known experimental lattice parameters of the NaTl-type phases the distance  $d_A$  [ $d_A = (a/4)\sqrt{3}$ ]. Pearson used instead of the radii, the diameters  $D_A$  and  $D_B$ , where  $D_A$  is always taken as the greater one, and plotted then a strain parameter  $(D_A - d_A)/D_B$  as function of diameter ratio  $D_A/D_B$ . He adjusted in the near-neighbor diagram also three lines calculated for 4 B-B, 4-4 A-B and 4 A-A contacts. In Pearson's original plot [40–43], there were seven data points obtained from the

binary phases known at that time LiAl, LiGa, LiIn, NaIn, and NaTl and – as mentioned above – also LiZn and LiCd. Pearson's five data points for the  $A^I B^{III}$  phases are plotted in the left lower part of Fig. 20, not considering LiZn and LiCd. The three left lower points belong to "InLi" (In is here the greater A, Li the smaller B), LiAl and LiGa, and, the two slightly upper ones, to NaTl and NaIn. These five points lie above the line for "4 B-B" indicating that these contacts are compressed [46]. For the remaining 14  $A^I B^{III}$  compounds, the lattice parameters with NaTl-type structure have been used, obtained at zero temperature and pressure by WIEN2k (without correction for thermal expansion). These data and the corrected radii  $r_{Al}$  and  $r_{B^{III}}$  [43, 44] were the input for Fig. 20. The following radii have been used:  $r_{Li} = 1.509$ ,  $r_{Na} = 1.858$ ,  $r_K = 2.323$ ,  $r_{Rb} = 2.493$ ,  $r_{Cs} = 2.678$ ,  $r_{Al} = 1.379$ ,  $r_{Ga} = 1.358$ ,  $r_{In} = 1.610$ ,  $r_{Tl} = 1.663$ , in Å [40, 43]. Such near-neighbor diagram is shown for such 19  $A^I B^{III}$  compounds in Fig. 20.

Nearly 40 years ago, between 1968 and 1973, it was out of imagination for Pearson [40–43] that an  $A^I B^{III}$  compound of composition KTl with the NaTl-type structure could be prepared experimentally. At that time, high pressure experiments with a DAC were quite "exotic." Pearson concluded that "in KTl, however, the radius ratio (about 1.40), is so much larger, that compression of the K atom in order to achieve full Tl–Tl contacts is no larger profitable for formation of the NaTl arrangement" [42]. And also: "... even the most favorable case of KTl the value of  $D_A/D_B = 1.397$  is too large for Tl–Tl contacts to be formed by compression of the K atoms" [47] and "potassium compounds do not have the NaTl structure since even for the largest group III element, thallium. . ." [41].

However, inspection of Fig. 20 shows that Pearson was only quite right at ambient pressure, but the data point for KTl with the NaTl-type structure lies only slightly below the line for 4 B-B contacts. This is an indication that the B-B contacts have to be stretched. In NaTl, itself, with a lattice parameter of  $a = 7.467$  (10) Å at ambient pressure (Table 14), there is a Tl–Tl distance of 3.23(1) Å. On the other hand, in KTl with  $a = 8.01$ (2) Å at ambient pressure (Table 15), the Tl–Tl distance is 3.47(1) Å. Therefore, the Tl–Tl distance in KTl has to be stretched by 7%.

Inspection of Fig. 20 shows also that the six data points from KTl to CsIn (with increasing  $D_A/D_B$ : KIn, RbIn, RbTl, CsTl) lie also on a line which could be obtained by extrapolation of Pearson's original five data points. However, this extrapolated line intersects the calculated line for 4 B-B contacts at approximately  $D_A/D_B = 1.3$ . Below  $D_A/D_B = 1.3$ , 4 A-A contacts have to be compressed, above this value 4 B-B contacts have to be stretched. It is evident from Fig. 20 that for the 19  $A^I B^{III}$  compounds considered here, the smallest deviation to the calculated line for 4 B-B contacts is obtained for KTl to CsIn. Indeed, here the calculated pressure to obtain the NaTl-type structure for KTl and CsIn is only 5 GPa. The line for NaAl to NaGa has a medium deviation to the calculated line for 4 B-B contacts with stabilization pressures of 25 and 5 GPa. The largest deviation to the line for 4 B-B contacts is found for KAl to CsGa. Here the stabilization pressure is 30 and 20 GPa. This indicates that for these compounds the importance of 4 B-B contacts is lowered, but that of 4-4 A-B contacts is increased.

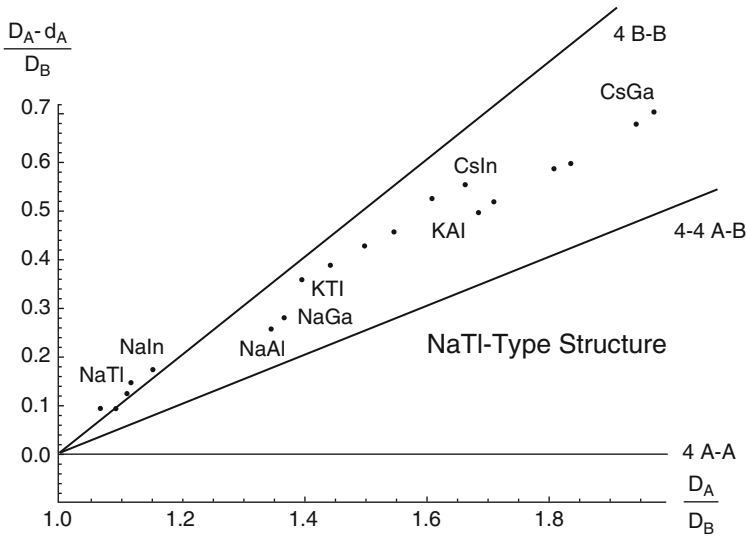


**Fig. 20** Near-neighbor diagram for the NaTl-type structure at 1 bar. The data for the ratio of the atomic diameters at 1 bar were taken from Teatum et al. [43, 44] and corrected for coordination number eight [41]

From the total energy  $E^o$  curves, discussed in Sects. 5.1–5.4, it was derived that LiAl ( $D_A/D_B = 1.094$ ), LiGa (1.111), InLi (1.067), and NaTl (1.117) (Fig. 20) could be suitable candidates for a high pressure transformation into the  $\beta$ -brass-type structure. For LiIn [20], the transformation into the  $\beta$ -brass-type structure was verified by DAC experiments in 1998. In this work, it was shown that for NaTl (1.117) (Fig. 14; Table 14) a  $\beta$ -brass phase could be obtained. For NaIn (1.154), the transformation pressure should be much higher. For LiAl (1.094) and LiGa (1.111), the HP transformations into the  $\beta$ -brass-type structure seem to be much easier.

## 6 Conclusion

The NaTl- and the  $\beta$ -brass-type structures in the 20 investigated  $A^I B^{III}$  compounds consist of interpenetrating cubes with 8:8 nearest neighbor coordination. Neglecting small differences, this is also true for the two tetragonal distortions. In the NaTl-type structure and its tetragonal distortion in space group  $I4_1/amd$ , 8:8 coordination is achieved for the  $A^I B^{III}$  compounds with 4 A-B contacts and, additionally, either with 4-4 A-A or 4-4 B-B contacts. In the ordered  $\beta$ -brass-type structure, the coordination consists of only 8:8 A-B contacts. The dimorphism of the NaTl- and the  $\beta$ -brass-type structures in a special compound depends on their total energies  $E^o$ . The WIEN2k calculations show that for small radius ratio  $r_A:r_B$ , the  $\beta$ -brass-type structure is favored, for large the NaTl-type structure. This ordering of the  $A^I$  and the  $B^{III}$  atoms in interpenetrating

cubes with 8:8 nearest neighbor coordination for both typically metallic structures can be changed by HP treatment.

As discussed in Sect. 4, the site occupation is identical for the NaTl- and the  $\beta$ -brass-type structure, and also its two tetragonal distortions, neglecting small differences. There are two interpenetrating cubes which give 8:8 nearest neighbor coordination. In the NaTl-type structure and its tetragonal distortion in space group  $I4_1/amd$ , this is achieved by 4-4 B-B and 4 A-B contacts, if the cube is B-centered, or by 4-4 A-A and 4 A-B contacts, if the cube is A-centered. In the  $\beta$ -brass-type structure and its tetragonal distortion in space group  $P4/mmm$ , the 8:8 nearest coordination is achieved by 8:8 A-B contacts.

Pearson had stated that the “NaTl-type structure is neither ionic nor dominated mainly by strong diamond-type covalent bonds, but characteristically metallic phases adopting 8-8 coordination” [43]. However, electron density calculations for KTI with the NaTl-type structure (Fig. 18) clearly show that even at 30 GPa covalent bonding in the four-connected net of Tl atoms is present. Up to 24.5 GPa no transformation of KTI ( $D_A:D_B = 1.397$ ) into the  $\beta$ -brass-type structure was observed in the DAC, and total energy calculations (Fig. 15) show that the energy difference between both structures is quite large.

For NaAl (1.347) and NaGa (1.368), the metallic radius of sodium seems also too large to obtain the  $\beta$ -brass-type structure in the same pressure range as above. The total energy  $E^0$  calculations with WIEN2k indicate that for larger  $D_A:D_B$  values (1.37–1.942) in comparison with  $\beta$ -brass-type structure, the NaTl-type structure is stabilized at pressures up to 30 GPa. The concurrence of the NaTl- and the  $\beta$ -brass-type structure is therefore strongly influenced by the ratio  $D_A:D_B$ .

For small  $D_A/D_B$  ratios (1.0–1.2), the transformation NaTl-type into the  $\beta$ -brass-type structure has been experimentally verified [20] in “InLi” ( $D_A:D_B = 1.067$  at 1 bar) and in NaTl by this work ( $D_A:D_B = 1.117$ ). Total energy  $E^0$  calculations show that it should be possible to perform this transformation in the pressure range up to 40 GPa also in LiAl ( $D_A:D_B = 1.094$ ) and in LiGa (1.111). Therefore, the  $\beta$ -brass-type structures for LiAl, LiGa, and NaTl, which could be obtained by applying high pressure up to 40 GPa, simulate the behavior of LiTl at 1 bar. This structural change, obtained “between” NaTl and LiTl by only lowering the metal radius of Na ( $r_{Na} = 1.858$  Å) to Li ( $r_{Li} = 1.509$  Å), can be understood by applying “high internal pressure” at 1 bar.

Phases with low  $D_A:D_B$  ratios achieving packing of  $A^I$  and  $B^{III}$  spheres either in the  $\beta$ -brass- or in the AuCu-type structure are energetically favored over those with covalent  $B^{III}$ – $B^{III}$  bonding in the NaTl-type structure. In addition, phases with an arrangement of  $A^I$  and  $B^{III}$  spheres should be more ductile (lower  $B_0$ ) than those with covalent  $B^{III}$ – $B^{III}$  bonding which should be more brittle (higher  $B_0$ ).

**Acknowledgments** The author thanks Prof. Dr. Peter Kroll, Department of Chemistry and Biochemistry, The University of Texas at Arlington, for support in the first stages of the WIEN2k calculations on  $A^I B^{III}$  compounds, when it became evident that contrary to earlier published data, LiIn with the  $\beta$ -brass-type structure is lower in energy than the NaTl-type structure. Prof. Kroll confirmed this result by own calculations with the program VASP. The author also thanks Prof. Dr. Peter Blaha, Institut für Materialchemie, University of Vienna, for critical comments and many advices.

## References

1. Zintl E, Woltersdorf G (1935) *Z Elektrochem* 41:876
2. Zintl E (1939) *Angew Chem* 1:52
3. Klemm W, Busmann E (1963) *Z Anorg Allg Chem* 319:297
4. Klemm W (1958) *Proc Chem Soc London*:329
5. Schäfer H, Eisenmann B, Müller W (1973) *Angew Chem* 85:742; *Angew Chem Int Ed* 12:694
6. Schäfer H (1985) *Ann Rev Mater Sci* 15:1
7. Hoffmann R (1988) *Solids and surfaces: a chemist's view of bonding in extended structures*. VCH Publishers, New York, p 3
8. Zintl E, Dullenkopf W (1932) *Z Physik Chemie B* 16:195
9. Schmidt PC (1985) *Phys Rev B* 31:5015
10. Corbett JD (2000) *Angew Chem* 112:682; *Angew Chem Int Ed* 39:670
11. Laves F (1941) *Naturwissenschaften* 29:244
12. Gottfried C, Schossberger F (1937) *Strukturbericht, Band III, 1933-1935*. Akademische Verlagsgesellschaft M.B.H, Leipzig, p 19
13. Zintl E, Neumayr S (1933) *Z Physik Chem B* 20:272
14. Zintl E, Brauer G (1933) *Z Physik Chem B* 20:245
15. Ewald PP, Hermann C (1931) *Strukturbericht 1913–1928*. Akademische Verlagsgesellschaft M.B.H, Leipzig, p 74
16. Maknovetskii AB, Krasko GL (1977) *Phys Stat Sol B* 80:341
17. Schmidt PC (1987) In: Clarke M, Chestnut H, Goodenough JB, Ibers JA, Evanston CK, Mingos DMP, Neilands JB, Palmer GA, Reinen D, Sadler PJ, Weiss R, Williams RJP (eds) *Structure and bonding, solid state chemistry*, vol 60. Springer Verlag, Berlin, p 91
18. Christensen NE (1985) *Phys Rev B* 32:207
19. Ehrenberg H, Pauly H, Hansen T, Jaud J-C, Fuess H (2002) *J Solid State Chem* 167:1
20. Schwarz U, Bräuninger S, Syassen K, Knip R (1998) *J Solid State Chem* 137:104
21. Evers J, Oehlinger G (2000) *Inorg Chem* 39:628
22. Dong Z, Corbett JD (1993) *J Am Chem Soc* 115:11299
23. Blaha P, Schwarz K, Madsen G, Kvasnicka D, Luitz J (2001) *WIEN2k: an augmented plane wave plus local orbital program for calculating crystal properties*, November 2001. Vienna University of Technology, Vienna
24. Blase W, Cordier G, Müller V, Häussermann U, Nesper R, Somer M (1993) *Z Naturforsch B* 48:754
25. Dong Z-C, Corbett JD (1996) *Inorg Chem* 35:2301
26. Mao H, Bell PM (1978) *Science* 200:1145
27. Mao HK, Bell PM, Shaner JW, Steinberg DJ (1978) *J Appl Phys* 49:3276
28. Rodriguez-Carvajal JR (1990) *FullProf: a program for Rietveld refinement and pattern matching analysis*. In: Abstracts of the satellite meeting on powder diffraction of XV congress of the IUCr, Toulouse, France, 1990. International Union of Crystallography, Chester, p 127
29. Sommer F, Fischer B, Predel B (1982) In: Borgstedt HU (ed) *Material behaviour and physical chemistry in liquid metal systems*. Plenum Press, New York, p 395
30. Miedema AR, Chatel de PF (1979) *Theory of alloy formation*. In: Bennett LH (ed) *Proceeding of a symposium of the AIME, annual meeting, New York 1980*, pp 344–387
31. Wu Z, Cohen R (2006) *Phys Rev B* 73:235116
32. Villars P, Calvert LD (1985) *Pearson's handbook for intermetallic phases*. ASM International, Materials Park, First Printing 1985
33. Villars P, Calvert LD (1988) *Pearson's handbook for intermetallic phases*. ASM International, Materials Park, Second Printing, February 1996
34. Murnaghan FD (1944) *Proc Nat Acad Sci U S A* 30:244
35. Perdew JP, Wang Y (1992) *Phys Rev B* 45:13224
36. Perdew JP, Burke S, Ernzerhof M (1996) *Phys Rev Lett* 77:3865

37. Zintl E, Brauer G (1935) *Z Elektrochem* 41:297
38. Zintl E, Dullenkopf W (1932) *Z Physik Chem B* 16:183
39. Massalski TB (1990) Binary alloy phase diagrams, vol 1: Ac-Ag to Ca-Zn. ASM International, Materials Park, p 178
40. Pearson WB (1968) *Acta Crystallogr B* 24:1415
41. Pearson WB (1969) In: Giessen BC (ed) Development in the structural chemistry of alloy phases. Plenum Press, New York, pp 45–48
42. McNeil MB, Pearson WB, Bennett LH, Watson RE (1973) *J Phys C Solid State Phys* 6:1
43. Pearson WB (1973) The crystal chemistry and physics of metals and alloys. Wiley-Interscience, New York, p 576
44. Teatum E, Gschneidner K, Waber J (1960) LA2345. US Dept of Commerce, Washington
45. Pearson WB (1973) The crystal chemistry and physics of metals and alloys. Wiley-Interscience, New York, p 151
46. Pearson WB (1973) The crystal chemistry and physics of metals and alloys. Wiley-Interscience, New York, p 53
47. Pearson WB (1973) The crystal chemistry and physics of metals and alloys. Wiley-Interscience, New York, p 578



Zintl Phases

Principles and Recent Developments

Fässler, Th.F. (Ed.)

2011, XI, 164 p. 73 illus., 40 illus. in color., Hardcover

ISBN: 978-3-642-21149-2